Nanoscale Advances

REVIEW

View Article Online
View Journal | View Issue



Cite this: *Nanoscale Adv.*, 2021, **3**, 2423

# A power-triggered preparation strategy of nano-structured inorganics: sonosynthesis

Zhanfeng Li,[a] Jun Dong,[a] Lun Wang,[a] Yongqiang Zhang,[bc] Tingting Zhuang,[a] Huiqi Wang,[a] Xuejun Cui[b] and Zonghua Wang*[a]

Ultrasound irradiation covers many chemical reactions crucially aiming to design and synthesize various structured materials as an enduring trend in frontier research studies. Here, we focus on the latest progress of ultrasound-assisted synthesis and present the basic principles or mechanisms of sonosynthesis (or sonochemical synthesis) from ultrasound irradiation in a brand new way, including primary sonosynthesis, secondary sonosynthesis, and synergetic sonosynthesis. This current review describes in detail the various sonochemical synthesis strategies for nano-structured inorganic materials and the unique aspects of products including the size, morphology, structure, and properties. In addition, the review points out the probable challenges and technological potential for future advancement. We hope that such a review can provide a comprehensive understanding of sonosynthesis and emphasize the great significance of structured materials synthesis as a power-induced strategy broadening the updated applications of ultrasound.

Received 14th January 2021
Accepted 5th March 2021

DOI: 10.1039/d1na00038a

rsc.li/nanoscale-advances



## 1. Introduction

Ultrasound, which is industrially generated from electrical energy by using a magnetostrictive or piezoelectric transducer,[1–4] often serves as a driving force to facilitate many physical, mechanical or chemical processes. Generally, high-frequency ultrasound is typically used in medical applications for diagnosis and therapy, *e.g.*, to aid in drug delivery, to break down blood clots, or even to destroy tumors in surgery.[5–9] By comparison, low-frequency ultrasound is widely used in research and industry to efficiently clean the debris from surfaces, to purify water from degrading contaminants, to initiate reduction, oxidation and hydrolysis reactions, or to accelerate crystallization and polymerizations.[10,11] For example, sonolysis or ultrasonic catalysis, as one of the advanced

[a]*Shandong Sino-Japanese Center for Collaborative Research of Carbon Nanomaterials, College of Chemistry and Chemical Engineering, Instrumental Analysis Center of Qingdao University, 266071 Qingdao, China. E-mail: lizhanfeng@qdu.edu.cn; wangzonghua@qdu.edu.cn*

[b]*College of Chemistry, Jilin University, 130012 Changchun, China*

[c]*Junan Sub-Bureau of Linyi Ecological Environmental Bureau, 276600 Linyi, China*

*Dr Zhanfeng Li is an associate professor at the College of Chemistry and Chemical Engineering of Qingdao University. He received his PhD degree in Applied Chemistry from Jilin University in 2016, under the supervision of Prof. Xuejun Cui. After joining Qingdao University, he worked as a Postdoctoral Research Fellow at the College of Materials Science and Engineering (Qingdao University), under the supervision of Prof. Zonghua Wang. His research interests focus on sonochemical synthesis, the design of new micro/nano-scale materials, and sonochemical applications in catalysis and biomedicine.*

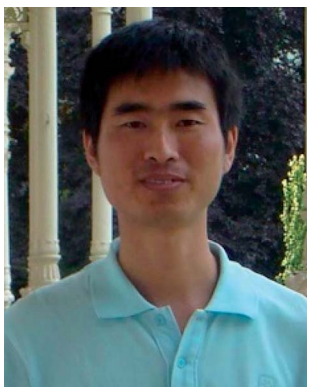

*Dr Xuejun Cui is a professor at the Department of Chemistry at the University of Jilin. He graduated in Applied Chemistry in 2003 and completed his PhD from Jilin University in 2008, under the supervision of Prof. Hongyan Wang. After that, he joined the faculty of the Chemistry Department in Jilin University. During the employment, he spent time as a junior research fellow at the Max Planck Institute of Colloids and Interfaces and Nanyang Technological University. His research interests focus on acoustic chemistry and the design and preparation of biomedical materials for drug delivery.*

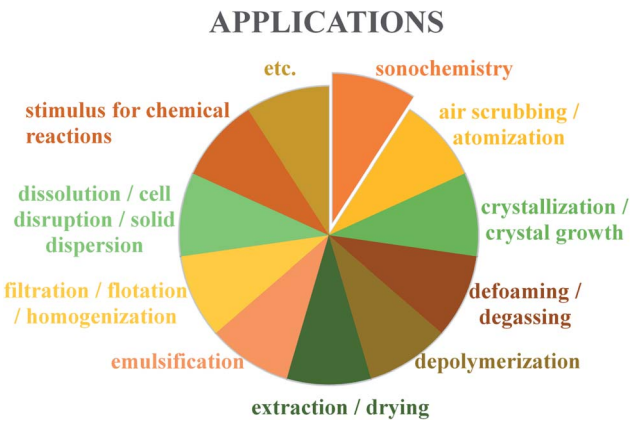


Fig. 1 General applications of ultrasound in chemistry, material, and manufacturing processes.

oxidation processes (AOPs), has been exploited for the degradation of toxic organics in order to protect the aqueous environment, where ultrasound irradiation combined with other AOPs and/or oxidizing agents can enhance the reaction rate, decrease the processing conditions, and reduce the overall energy consumption.[12,13] Fig. 1 lists the general applications of low-frequency ultrasound in chemistry, material, engineering and manufacturing fields, and many processes refer to the chemical effects from ultrasound. As for the chemical effects from ultrasound irradiation, the precise term "sonochemistry" is coined, covering a special research area where powerful ultrasound induces chemical reactions or even merely participates in some chemical processes as a nonclassical method.[14,15] Actually, since ultrasonic equipment came into being, the chemical effects from ultrasound or sonochemistry-based applications have been reported,[16] and especially, more and more ultrasound-assisted methods have emerged in synthetic chemistry, organometallic chemistry, material chemistry, biological chemistry, medical chemistry, *etc.*[17–23]

Inorganic materials have attracted much attention owing to their unique structures and/or properties and widespread applications in many fields ranging from catalysis, hydrogen storage, and energy storage to the sensors, electronics, biotechnology and nanomedicine, and correspondingly, numerous methods have been developed for their synthesis, such as the coprecipitation method, sol–gel method, and solvothermal method.[24–27] So far, many sonochemical preparation methods including a few combined strategies with the aid of ultrasound irradiation have been also carried out to create inorganic materials, where ultrasound irradiation seems to be a power-inducing preparation source. Recently, we have published a review paper on the catalytic applications of ultrasound-synthesized inorganic nano-materials, and the content highlighted sonochemistry applications in the inorganic-based catalysis processes including reduction, oxidation, degradation, polymerization, *etc.*[4] In contrast, this review will provide an overview on the latest developments of the ultrasound-assisted synthesis of nano-structured inorganics, where more emphasis is put on the matters about the sonosynthesis (or sonochemical synthesis), wherein it will provide a fundamental understanding of the basic principles of sonosynthesis including acoustic cavitation, sonochemistry, and physical/mechanical effects and will present the nano-scale inorganic materials produced by the sonochemistry-inducing synthesis, as well as the size, morphology, structure, and properties of products. Moreover, the review will point out the prospective challenges and trends in sonosynthesis-assembled programming of miscellaneous materials, broaden the synthetic methodology, and conclude the significance of sonosynthesis in abundant applications.

## 2. Mechanism of sonosynthesis

For either low-frequency or high-frequency ultrasound, sonosynthesis is a conventional representation for chemical reactions. Theoretically, there is no direct interaction at least in a molecular level between ultrasound and chemical species, since some typical index values of sound wave are much larger than the molecular scale in a liquid system, *e.g.*, sound velocity (1000–1500 m $s^{-1}$) and sound wavelength ($10^{-6}$ to $10^{-1}$ m).[28,29] In comparison to other energy sources such as heat, light and microwave, ultrasonic irradiation can offer some extreme transient conditions (*e.g.*, localized high pressure and temperature) by acoustic cavitation and bring up some interesting chemical effects on the synthesis processes,[30] or taken as a whole, the sonochemistry as well as the derivative sonosynthesis originates from acoustic cavitation primarily.

Acoustic cavitation, namely the continuous changing states of cavitation bubbles including the formation, growth, and violent collapse, is a transient process caused by irradiating a liquid with ultrasound.[31] The ultrasound, as a conventional pressure wave, can cause the liquid medium to experience an alternate compression and rarefaction phase when moving forward, and the particles in the liquid will respond to the acoustic pressure cycles, resulting in sound propagation. During the rarefaction phase (or negative-pressure) cycle, the liquid is pulled apart at some sites containing some gaseous impurities (known as "weak spots") by overcoming intermolecular interactions and the cavitation bubbles are usually

*Prof. Zonghua Wang is a Group Leader at the Department of Chemistry, University of Qingdao. She obtained her M.S. degree in Analytical Chemistry from the China University of Geosciences in 1987 and accomplished her PhD in Analytical Chemistry from Tsinghua University in 2004, under the supervision of Prof. Guoan Luo. Her current research interests include the functionalization and application of nanomaterials, nanoanalytical chemistry, electroanalytical chemistry, and biofunctional interfaces and materials.*

nucleated at the "weak spot" sites.[32] Once formed, the bubbles can keep trapped in the acoustic pressure field and grow through a rectified diffusion process owing to the contributing area and shell effect. The average surface area of cavitation bubbles during the rarefaction phase is larger than during the compression phase, so there is always a gas flow into the bubbles over several cycles. Meanwhile, the gas inflow is always higher during the expansion stage because the diffusion rate into the cavity should be proportional to the concentration gradient of solvent vapor and dissolved gas, so such a concentration gradient in the fluid shell around the bubbles also contributes to the bubble growth in volume. When the bubbles grow up to a critical size range (typically tens of micrometers), they will be no longer stable and undergo a rapid inertial overgrowth by coupling strongly to the acoustic field, and subsequently, a catastrophic collapse occurs at some point. During the cavitation, the compression of oscillating bubbles accumulating ultrasonic energy effectively leads to an enormous energy concentration being stored within a small volume. The concentrated energy will be released from the bubbles within a very short time (estimated 3.5 μs) *via* an implosive collapse that is a nearly adiabatic process, and thus, acoustic cavitation can result in the formation of a localized micro-scale "hotspot" which experiences high temperature (up to thousands of degrees) and high pressure (over hundreds of atmospheres).[33–36] Fig. 2 gives us the schematic illustration of hotspot formation under acoustic cavitation. The intensity of acoustic cavitation, largely determining the rate and/or productivity of sonosynthesis, can be simultaneously influenced by the ambient conditions (*e.g.*, dissolved gases, solvent, reaction temperature, and hydrostatic pressure) and the device parameters (*e.g.*, ultrasonic frequency and acoustic power), and the inductive description can be presented as follows: (1) the dissolved gases significantly act as the "weak spot" sites in a liquid, but the bubbling gases can produce more cavitation bubbles through the mixture, and the type of bubbling gases is important as well; for instance, the gas with a higher specific heat ratio should give a greater cavitation effect, while the gas with a larger solubility provides more nucleation sites for cavitation.[37,38] (2) The cavities may be more readily formed when a solvent has higher vapor pressure, lower viscosity and surface tension, but the one with opposing characteristics benefits the cavitation intensity, so an optimum solvent is able to dominate the cavitation.[28] (3) In a certain system, an increasing ambient temperature may lead to more favorable results, but has a negative effect on the sonochemical effects, namely, higher ambient temperature results in easier bubble formation, whereas the bubbles containing more vapors receive an overall decrease in the cavitation.[16] (4) Contrary to the temperature, enlarging the ambient pressure of the system generally leads to a predominant increase in acoustic cavitation as a result of the decrease in vapor pressure. (5) Ultrasonic frequency can alter the critical size of the formed cavitation bubbles, and low frequency produces more violent cavitation with higher localized temperature and pressure.[16] (6) When a continuously advancing ultrasonic power is delivered to the reaction system, the acoustic cavitation will increase to a maximum and then decrease probably because the dense cavitation bubbles formed near the probe tip at high power acts to block the energy transmitted from the probe to the fluid.[16]

To date, several competing theories have been postulated to explain the chemical effects created by ultrasound irradiation, but most of them are completely discarded as a valid mechanism of sonoluminescence and sonochemistry.[39,40] Since the acoustic cavitation accounts for the transient characteristic conditions, hotspot theory has become more generally accepted, where it highlights that the extreme conditions from the localized hotspots will form a few active species for the follow-up sonochemistry. In a system, the bulk of the liquid has no direct sonochemical events, but the compressional heat released from collapsing bubbles generates enough high temperatures effectively and locally inducing the dissociation of chemical bonds, and the induced radicals may diffuse into the liquid prior to further reactions. Primary sonochemistry refers to the indiscernible processes that result in the formation of radical species from the volatiles and/or gases inside the collapsing bubble. In the bubble center (Fig. 3), namely at the hotspots, the harsh conditions can cause the sonolysis reaction

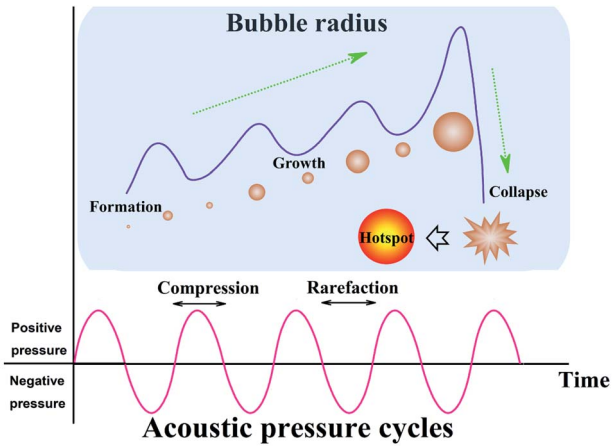


Fig. 2 Schematic illustration of the hotspot formation under acoustic cavitation.

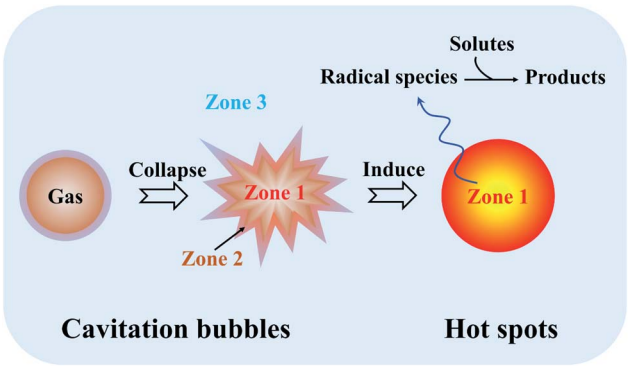


Fig. 3 Schematic illustration and reaction zones of primary sonochemistry and secondary sonochemistry.

to occur, where the gases present in the bubbles (Zone 1) or in the interfacial region (Zone 2) between the bubble center and bulk liquid will experience large gradients of temperature, pressure, and shear. As a powerful tool to understand the origin of the drastic conditions created by acoustic cavitation, the analysis of sonoluminescence spectra from water under power ultrasound reveals the overpopulation of $OH(A^2\Sigma^+)$ vibrational levels, indicating the formation of non-equilibrium plasma inside the cavitation bubbles.[40] The non-equilibrium plasma is the major state of gas inside violently collapsing cavitation bubbles. Based on a two-site model for the sonochemical regions, most of the radical production is thought to occur in the interior vapor phase when the liquid layer immediately surrounding the cavitation bubbles bursts into the bubbles upon the cavitation collapse. Moreover, the primary sonochemical effect relates to the cavitation bubble types. The transient cavitation bubble often grows to a large size quickly and collapses after one acoustic cycle, which accounts for most of the chemical activity in the system. The stable cavitation bubble can persist for more acoustic cycles and create a large shear gradient when it collapses, where the shear force plays an important role in a sonochemical system, *e.g.*, the emulsification caused by the cavitation is significant to allow an efficient preparation of polymer microspheres.[41]

Different from primary sonochemistry, secondary sonochemistry involves that the initial species formed in the primary sonochemical stage migrate into the surrounding liquid and suffer from a variety of reactions with solutes (Zone 3). In the well-studied case of sonicating aqueous liquids (Fig. 4), the fragmentation of water can generate highly active hydrogen radicals ($H^{\bullet}$) and hydroxyl radicals ($^{\bullet}OH$) (reaction 1), which has been captured photographically by using a luminol solution to enhance the blue sonochemiluminescence generated near the cavitation bubbles.[42] Upon diffusing out, these $H^{\bullet}$ and $^{\bullet}OH$ radicals can combine to produce hydrogen ($H_2$) and hydrogen peroxide ($H_2O_2$) (reactions (2) and (3)) if taking no account of their recombination to be an original form or can also generate secondary radicals ($R^{\bullet}$) (reaction 4) by reacting with organic additives (*e.g.*, 2-propanol or ethanol) or produce hydroperoxyl radicals ($HO_2^{\bullet}$) by combining with dissolved oxygen ($O_2$) (reaction 5). Either the strong oxidants or reductants are used to initiate various chemical reactions in an aqueous or nonaqueous solution including the reductions, oxidation, hydroxylation of organics, *etc.*[43] Like the acoustic cavitation, the generation of radicals strongly depends on a great number of factors. Take ultrasound frequency as an example, the production of active species stays at a very low level under a low-frequency ultrasound even though the collapse of larger cavitation bubbles creates stronger shear forces, and with the frequency enhancing, the production rates increase quickly up to a maximum at 300–800 kHz and then drop off, where the shear force decreases considerably.

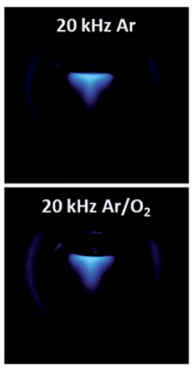


$$H_2O \rightarrow H\bullet + \bullet OH \quad (1)$$

$$2H\bullet \rightarrow H_2 \quad (2)$$

$$2\bullet OH \rightarrow H_2O_2 \quad (3)$$

$$RH + \bullet OH\ (\text{or } H\bullet) \rightarrow R\bullet + H_2O\ (\text{or } H_2) \quad (4)$$

$$H\bullet + O_2 \rightarrow HO_2\bullet \quad (5)$$

Fig. 4 Sonochemiluminescence (left) observed in a luminol solution (pH 11.0, $Na_2CO_3$) under ultrasound irradiation (20 kHz, 33 W), in which the sonolysis of water involves several rapid primary and secondary reactions (right). Reproduced with permission.[42] Copyright 2018 American Chemical Society.

For many materials synthesis or other relevant events, the sonochemical processes of solvents or solutes serve as an excitation source and induce some catalysis or sonosynthesis which is a power-inducing preparation strategy. Besides, ultrasound irradiation often gives rise to numerous physical effects (*e.g.*, simple heating, shock waves and microjets) accompanied by the chemical consequences, and these factors are able to order the sonosynthesis performance in materials synthesis by affecting the frequency and efficiency of chemical reactions.[44] During sonication, the typical ultrasonic horns deliver acoustic energy into the liquid, changing into heat, which can be useful for activating reactive atoms or molecules, accelerating dissolution and facilitating crystallization. The microjets occur due to the asymmetrical collapse of highly energetic bubbles in any heterogeneous system, and they can lead to the modification of surfaces (pitting and erosion) or the generation of surface nanostructures.[36,45] Shock waves will be created if a bubble unperturbed by the surface rebounds rapidly from its minimum spherical radius causing the compression of the surrounding liquid to propagate outwards.[46,47] The shock waves can induce several different mechanical, physical or chemical consequences, *e.g.*, increasing the mass transport due to strong turbulent mixing and acoustic streaming, accelerating solid particles suspended in the liquid, and inducing changes in size distributions, morphologies and surface compositions owing to the enhanced interparticle collisions. Additionally, the mechanical effects (*e.g.*, shear force, interparticle collisions, rapid mixing, and turbulence) from ultrasound irradiation are also important in the chemical consequences. Anyhow, the applications of sonosynthesis almost cover the chemical, physical and/or mechanical effects, for example, the fragmentation for brittle materials, the emulsification for immiscible liquids, the agglomeration for malleable materials, the exfoliation of layered materials into 2D layers, and even the fabrication and delivery of drug systems.[48,49]

## 3. Synthesis of inorganic nanomaterials

So far, the synthesis of inorganic nanomaterials has been explored with a view to the nature of precursors, the structures and properties of products and the feasibility and simplification

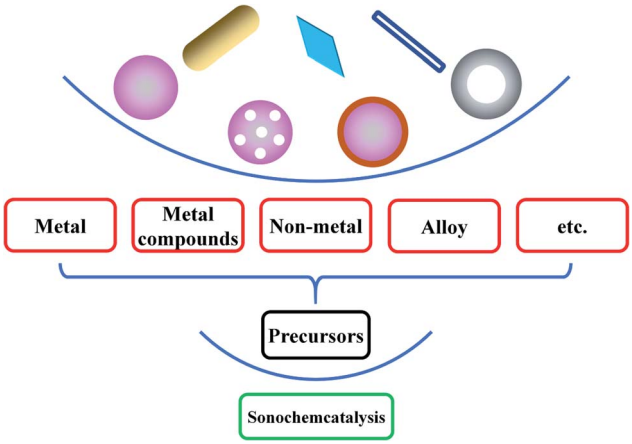


Fig. 5 A variety of inorganic nanomaterials based on sonocatalysis.

of methods. For instance, Sun *et al.* successfully prepared a $GdMnO_3$ material using a typical sol–gel method and subsequently *in situ* generated $GdMn_2O_5/GdMnO_3$ materials by acid treatment for complete oxidation of oxygenated VOC;[50] Tan *et al.* synthesized $TiO_{2-x}/W_{18}O_{49}$ with core–shell or double-shelled hollow microspheres through a facile multi-step solvothermal method, where the advanced architecture significantly enhanced the electronic properties of $TiO_{2-x}/W_{18}O_{49}$ for $CO_2$ photo-reduction efficiency;[51] Deng and co-workers fabricated $TiO_2$ supported Pt nano-/single-atom catalyst by using the molten salt method, and 0.2 wt% Pt catalyst showed high catalytic activity for toluene removal.[52] Our team once created superparamagnetic ferroferric oxide nanoparticles by the coprecipitation method and then yielded hydrophilic or hydrophobic targeting biomaterials by a few modifications.[53] As a supplementary choice, ultrasound irradiation provides a facile route for the synthesis of the nanomaterials, mainly attributed to primary sonosynthesis, secondary sonosynthesis and synergetic sonosynthesis, where primary sonosynthesis is based on primary sonochemistry when secondary sonosynthesis widely employs the secondary sonochemical consequences. Many inorganics including metals, alloys, metal compounds (*e.g.*, metal oxides, metal sulfides, and metal nitrides), and non-metals (*e.g.*, carbon materials, silicon materials, and selenium materials) have been yielded from the precursors, widely covering a variety of structures such as solid structures, hollow structures, core–shell structures, porous structures, nanotube structures, nanorod structures, and layered structures (Fig. 5).

## 4. Primary sonosynthesis

Primary sonosynthesis derives from the case that the implosive collapse of cavitation bubbles releases the stored energy within a very short time in a nearly adiabatic way so that the surrounding solvent or solutes experience high temperature inducing the breakage of chemical bonds. Some cases on the primary sonosynthesis have been summarized in Table 1. Directly, such sonosynthesis sometimes does not involve the quadratic transformation of active species. A few volatile organometallic compounds in a nonvolatile solvent such as silicone oil or long-chain hydrocarbons can cause the dissociation of organic groups and the release of individual metal atoms under ultrasound irradiation. Under argon gas, the sonication of $Fe(CO)_5$ in an alkane solvent or ionic liquid with a low vapor pressure efficiently yielded a black porous iron powder with traces of residual carbon and oxygen at the freezing point.[54] In the process, the atoms of the organometallic compound were thermally excited to the point where visible light was emitted analogous to the emission from flame excitation. Certainly, the nonvolatile solvents were needed because the additional vapor had to absorb the available energy in the collapsing bubble in order that the achieved conditions were much less extreme. Because the metal atoms were so rapidly cooled that crystallization was prevented within a short-lifetime cavitation event, the obtained product appeared to be an agglomeration of 20 nm amorphous nanoparticles. Other metal precursors with single or multiple ligands like $Cr(CO)_6$, $Ni(CO)_4$ and $Co(CO)_3NO$ also have produced amorphous porous metal nanoparticles, even obtaining alloy nanoparticles by varying the composition in the solution.[55]

Under the high-temperature conditions provided by the hotspots, the metal atoms decomposed from volatile organometallic compounds are highly active and can react with dissolved gas in the solvent to form new nanomaterials, for example, $Mo(CO)_6$ in hexadecane and $W(CO)_6$ in diphenylmethane by sonochemically heating under $CH_4/H_2$ gas separately led to the formation of nanostructured $Mo_2C$ or $W_2C/C$ porous aggregates, and the products showed superior activity, selectivity and stability for the dehydrogenation and/or hydrodehalogenation of organic pollutants.[56,57] Alternatively, some metal nitrides or metal oxides were also produced when the sonication of metal carbonyl compounds occurred under a reductive $NH_3/H_2$ gas mixture or in the presence of air.[58] Under ambient air of 80 °C, Argirusis *et al.* used organic solvents containing the precursors $W(CO)_6$ or $Mo(CO)_6$ to sonochemically prepare metal oxide nanoparticles on anode materials[59] and revealed that the size distribution and morphology of nanoparticles responded to ultrasound intensity and solvents when their decoration loading extent on substrates was affected by ultrasound intensity/duration as well as the ratio of precursor and substrate compounds. Interestingly, Zavala-Rivera *et al.* carried out the sonochemical reaction of $Fe(CO)_5$ in octanol under an inert air condition or pure oxygen condition using low-intensity ultrasound with a frequency of 40 kHz[60] and finally obtained iron carbide@iron oxide nanoparticles composed of an iron carbide core and a magnetite shell. Based on the core–shell structure, researchers concluded a possible sonosynthesis mechanism that the formation of the iron oxide layer occurred *via* the secondary interaction of iron carbide and oxygen followed by the decarbonization of $Fe(CO)_5$ to produce the nucleation points of iron carbide with the aid of oxygen.

The sonochemically released metal atoms are also able to react with other solutes or even solvent molecules. When the Fe atoms were released from the $Fe(CO)_5$ precursors under ultrasound irradiation, individual smaller iron nanoparticles with 8 nm diameter would be created if oleic acid or other similar

Table 1 Synthesis based on the primary sonocatalysis

| Precursor | Product | Experimental parameters under ultrasound | Ref. |
|---|---|---|---|
| $Fe(CO)_5$ | Porous iron | Decane, Ar atmosphere, 20 kHz, 100 W $cm^{-2}$, sonication for 3 h | 54 |
| $Mo(CO)_6$ | $Mo_2C$ | Hexadecane (50 mL), Ar atmosphere, 20 kHz, 100 W $cm^{-2}$, 90 °C, sonication for 3 h | 56 |
| $W(CO)_6$ | $W_2C$/C | Diphenylmethane (50 mL), 20 kHz, 600 W, 32 W $cm^{-2}$, 80 ± 2 °C, sonication for 30 min | 57 |
| $Fe(CO)_5$ | $Fe_{2-3}N$ | Decane, $NH_3/H_2$ (3.5 : 1), 20 kHz, 100 W $cm^{-2}$, 0 °C, sonication for 4 h | 58 |
| $W(CO)_6$ or $Mo(CO)_6$ | WOx or MoOx | Diphenylmethane and decalin (100 mL), ambient air, 20 kHz, 200 W, 80 °C, sonication for 3 h | 59 |
| $Fe(CO)_5$ | Iron carbide@iron oxide core–shell nanoparticles | Oleic acid, 1-octanol (5 mL), 40 kHz, room temperature, sonication for 40 min | 60 |
| $Fe(CO)_5$ | Iron colloid of Fe/FeO | Oleic acid, hexadecane, Ar atmosphere, 40 kHz, 30 °C, sonication for 1 h | 61 |
| $Mo(CO)_6$ | Clustered $MoS_2$ nanoparticles | Elemental sulfur, 1,2,3,5-tetramethylbenzene, Ar atmosphere, 20 kHz, 80 W $cm^{-2}$, 80 °C, sonication for 1.5 h | 63 |
| $Cu(CH_3COO)_2 \cdot H_2O$, $Co(NO_3)_2 \cdot 6H_2O$, $Ni(NO_3)_2 \cdot 6H_2O$ | Nano-sized Cu(II), Co(II) and Ni(II) complexes | Ahpv ligand, ethanol (10 mL), 24 kHz, 400 W | 64 |
| $CuCl_2$ | $[Cu(L)(H_2O)Cl]$ | 2-((Pyridin-3-ylmethylene)amino) phenol (HL), MeOH (10 mL), 40 kHz, 400 W | 65 |
| $Pb(NO_3)_2$ | $[Pb(L)(SCN)_2]_n$ | l-Methylimidazole (L), KSCN, methanol, 60 W, 30 °C, sonication for 30 min | 66 |
| Gallium | Ga@C-dots | Decane, dodecane, hexadecane or polyethylene glycol, 20 kHz, 750 W, 50 °C or 60 °C, sonication for 3–180 min | 67 and 68 |
| $Mo(CO)_6$ | $MoO_3$-coated silica nanoparticles, hollow $MoS_2$ | Silica spheres, elemental sulfur, isodurene, Ar atmosphere | 69 |
| $Co_4(CO)_{12}$ | Porous $Co_3O_4$ | Carbon nanotubes, hexane, sonication for 0.5 h | 70 |
| $Fe(CO)_5$ | Hollow hematite | Carbon nanoparticles, hexadecane (40 mL), argon flow, 20 kHz, 50 W $cm^{-2}$, 20 °C, sonication for 3 h | 71 |
| $Si_3H_8$ | Silicon nanoparticles | $N_2$-filled atmosphere with residual traces of $H_2O$ and $O_2$ (~1 ppm), 26 kHz, 32–130 W $cm^{-2}$, 1–4 W, 25–40 °C, sonication for 2 min | 72 |
| *p*-Xylene | Single-walled or multi-walled carbon nanotubes | Silica powder, ferrocene, *p*-xylene solution (50 mL), pulsed 65% at 200 W, atmospheric pressure, room temperature, sonication for 20 min | 74 and 75 |
| Dopamine hydrochloride | Nitrogen-doped carbon quantum dots | Dimethylformamide (150 mL), 20 kHz, 600 W, sonication for 8 h | 76 |

surfactants were present in the solvent to stabilize the metal atoms.[61] To prepare the coated iron nanoparticles, Nikitenko *et al.* reported the sonochemical decomposition of iron carbonyl indiphenylmethane, where an air-stable magnetic powder was formed after annealing the as-prepared sample at 973 K in argon.[62] The nanoparticle structure featured a core–shell geometry consisting of an $Fe_3C$ layer (about 3 nm thickness) on the top of a crystallized Fe core, and the ratio of Fe to $Fe_3C$ was close to 4 : 1. Other core–shell transition metal nanoparticles have been also created in the similar way, but some syntheses were usually particular and limited.[3] In an ultrasound process reported by Suslick *et al.*, adding elemental sulfur to the 1,2,3,5-tetramethylbenzene containing $Mo(CO)_6$ produced clustered $MoS_2$ nanoparticles with a higher edge

 

surface area under argon gas,[63] and such $MoS_2$ nanoparticles substantially exhibited high catalytic activity for the hydrodesulfurization of thiophene. Abdel-Rahman *et al.* once synthesized a Schiff base ligand (ahpv) by the condensation of 3-methoxysalicylaldehyde and 2-amino-3-hydroxypyridine and then added it dropwise to the ethanol solutions of different metal salts (*i.e.*, $Cu(CH_3COO)_2 \cdot H_2O$, $Co(NO_3)_2 \cdot 6H_2O$, and $Ni(NO_3)_2 \cdot 6H_2O$) positioned under high-density ultrasound irradiation, preparing nano-sized Cu(II), Co(II) and Ni(II) complexes of ahpv.[64] Rayan *et al.* obtained another nano-sized Schiff base ligand copper complex $[Cu(L)(H_2O)Cl]$ by using the sonochemical route, where L was 2-((pyridin-3-ylmethylene) amino)phenol prepared by the condensation of 3-pyridinecarboxaldehyde with 2-aminophenol.[65] In a study of Hayati *et al.*,[66] novel metalorganic coordination polymer compounds were fabricated with the aid of the sonochemical process, in which l-methylimidazole (L), KSCN and $Pb(NO_3)_2$ were used to synthesize $[Pb(L)(SCN)_2]_n$ by a branch tube method under high-density ultrasound. Gedanken *et al.* applied ultrasound irradiation of molten gallium in various organic liquids to produce some identified nanometric gallium particles,[67,68] *e.g.*, gallium spheres coated with a carbon film when gallium was sonicated in decane, dodecane and hexadecane, precipitated gallium particles coated with C-dots and supernatant gallium-doped C-dots during the sonication of gallium in polyethylene glycol. After investigating the nature of the product, they found that the ultrasound irradiation of molten gallium immersed in organic liquids caused the partial decomposition of the hydrocarbon medium prior to the interaction between carbon and gallium.

In addition, a removable template (*e.g.*, $SiO_2$ nanoparticles or microspheres) present can give an aid to the produced free metal atoms to directly deposit onto the support when sonicating the volatile organometallic precursors, forming different structured materials. Under the air, the ultrasound irradiation of $Mo(CO)_6$ and silica nanoparticles in 1,2,3,5-tetramethylbenzene yielded $MoO_3$-coated silica nanoparticles which would leave hollow $MoO_3$ behind by using HF to etch the silica component, and instead, adding elemental sulfur into the system and replacing the air with Ar gas could form hollow $MoS_2$ (Fig. 6).[69] Except the $SiO_2$ materials, carbon nanoparticles and organic ligands can also serve as a sacrificial template to inorganic nanomaterials. The sonochemical product of $Co_4(CO)_{12}$ in the presence of carbon nanotubes would not be amorphous cobalt but porous $Co_3O_4$,[70] where the carbon nanotubes as a template spontaneously removed themself *via* the combustion attributed to the rapid oxidation of elemental Fe upon air exposure. In a similar fashion, the precursor $Fe(CO)_5$ also could produce hollow hematite when carbon nanoparticles were employed as a template.[71]

In addition, nonmetal precursors are able to facilely and highly produce amorphous nanomaterials by the sonosynthesis effects. Bedini *et al.* carried out the sonochemical synthesis of

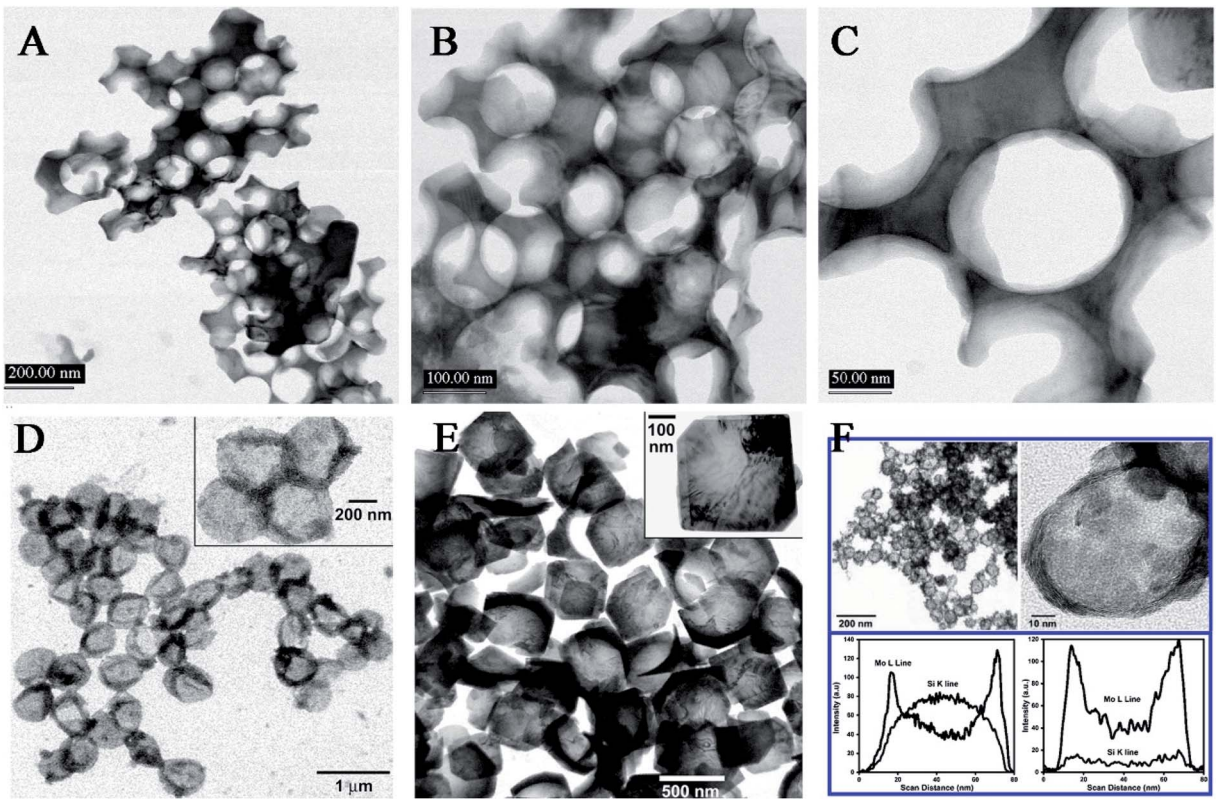


Fig. 6 TEM micrographs of conventionally prepared silica-templated $MoO_3$ (A, B, C); TEM micrographs of sonochemically prepared hollow $MoO_3$ nanospheres before (D) and after (E) thermal annealing thermal annealing at 350 °C, where insets show higher magnification; TEM micrographs of sonochemically prepared hollow $MoS_2$ nanospheres after thermal annealing at 450 °C, and EDX line analysis across the single $MoS_2/SiO_2$ and hollow $MoS_2$ (F). Reproduced with permission.[69] Copyright 2005 American Chemical Society.

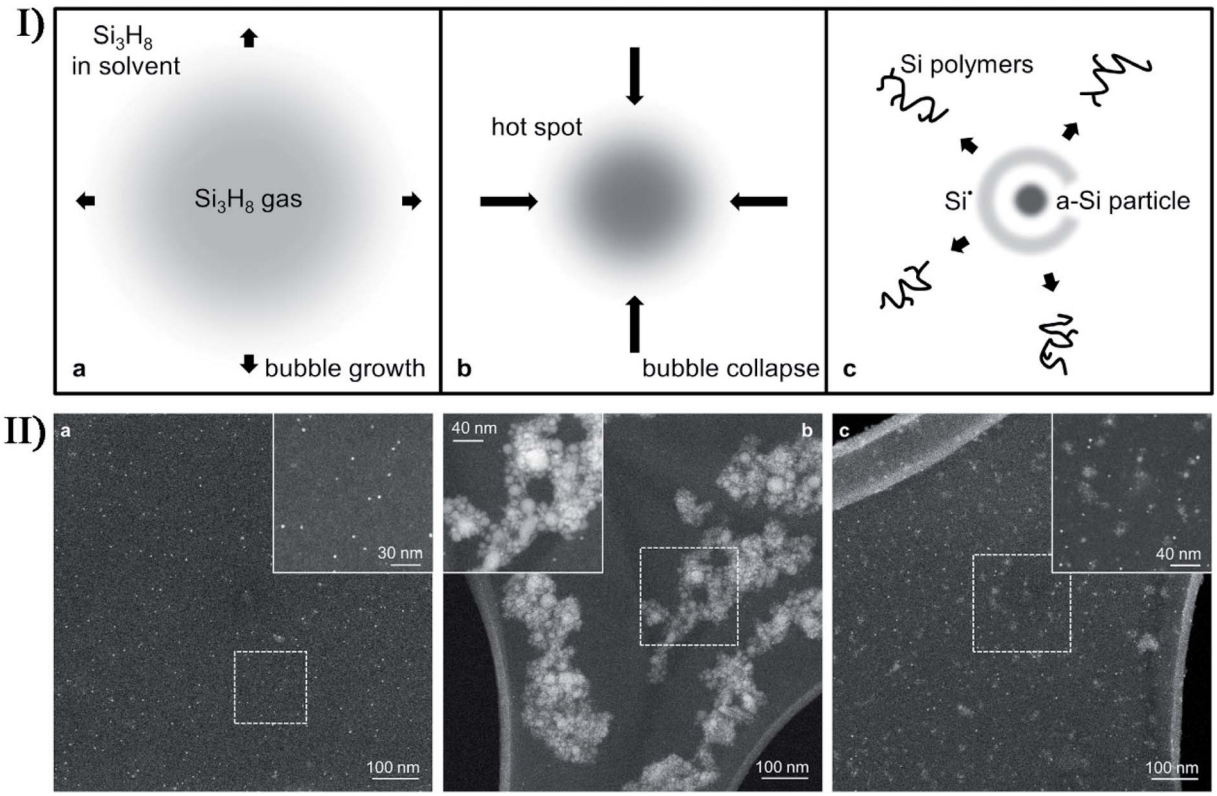


Fig. 7 (I) Schematic depiction of the growth and collapse of a bubble and the ensuing sonochemical effects enabling the synthesis of solid-state silicon: (a) during decompression cycles, an expanding bubble is preferentially filled with highly volatile trisilane ($Si_3H_8$); (b) upon bubble collapse, high transient temperatures and pressures result in the creation of a "hot spot"; (c) the implosion results in the generation of new silicon-containing species, namely an amorphous silicon (a-Si) particle, Si radicals (Si•), and Si polymers. (II) Dark field STEM images depicting the effects of sonication conditions on Si-nanoparticle production: (a) monodisperse Si-nanoparticles synthesized with low tip amplitude ($A = 48$ μm) and high trisilane concentration (47 wt%); (b) larger Si-nanoparticles synthesized with both high A (192 μm) and high trisilane concentration; (c) blend of Si-nanoparticles synthesized with high A and low trisilane concentration (1 wt%). The insets show higher resolution images of the regions enclosed by the dashed boxes. Reproduced with permission.[72] Copyright 2017 Elsevier.

silicon nanoparticles,[72] where the trisilane ($Si_3H_8$) solution underwent the sonication process in an inert $N_2$ atmosphere with residual traces of $H_2O$ and $O_2$. The as-synthesized silicon nanoparticles were discrete, hydrogenated, and non-crystalline. Therefore, the isolated formation of nanoparticles was attributable to the interplay among the extreme conditions during bubble collapse and the high density of active species (*e.g.*, silicon radicals) created at such spatially localized points (Fig. 7), while the amorphous morphology was ascribed to the residual bonded hydrogen in the particles due to incomplete diffusion during the short-lived collapse and the proposal that the silicon matrix did not have enough interaction time to reconstruct into a crystalline state. The silicon nanoparticles had a tunable size in the range of 1.5–50 nm, which could be controlled by varying the ultrasound amplitude or the trisilane concentration. Researchers found that low ultrasound amplitude or low trisilane concentration favored the generation of discrete and monodisperse silicon nanoparticles, which might be attributed to smaller microbubbles and/or less trisilane in-diffusion during bubble growth. Correspondingly, high amplitude and high trisilane concentration produced large amounts of larger and more polydisperse particles. In the absence of any templates or surfactants, the sonication of amorphous selenium colloids in alcohol could thermodynamically form trigonal selenium nanowires through a solid-solution-solid transformation mechanism,[73] where selenium nanocrystals were sonochemically nucleated in a trigonal structure and acted as the seeds of nanowires. Other nonmetal nanomaterials, such as graphene quantum dots, black phosphorus quantum dots and carbon nanodots, can be also prepared from the sonication of the corresponding precursors. When ultrasound was used to irradiate a *p*-xylene solution containing silica powder and ferrocene, *p*-xylene would be pyrolyzed to carbon atoms or moieties by the catalytic Fe clusters sonochemically decomposed from the ferrocene and finally produce high-purity, single-walled or multi-walled carbon nanotubes on the nucleation sites provided by silica powder.[74,75] Lately, Zhou *et al.* fabricated nitrogen-doped carbon quantum dots with temperature-dependent fluorescence by ultrasonic treatment of dopamine in dimethylformamide; moreover, the fluorescence had a sensitive quenching phenomenon towards $Fe^{2+}$ ions.[76]

## 5. Secondary sonosynthesis

Apart from primary sonosynthesis, secondary sonosynthesis significantly or more assists in the synthesis of inorganic

 

Table 2 Secondary sonocatalysis synthesis of nanostructured metals from the nonvolatile precursors

| Precursor | Product | Experimental parameters under ultrasound | Ref. |
|---|---|---|---|
| $HAuCl_4$ | Au nanoparticles | Aqueous solution (70 mL or 200 mL), 1-propanol, argon atmosphere, $0.1 \pm 0.01$ W $mL^{-1}$, 20–1062 kHz, 21 $\pm$ 2 °C | 78 |
| $HAuCl_4$ | Au nanorods and nanoparticles | Aqueous solution (60 mL), CTAB, $AgNO_3$, ascorbic acid, pH 3.5, argon atmosphere, 200 kHz, 200 W, 27 °C | 79 |
| $HAuCl_4$ | Au nanodecahedra | PVP/DMF solution (15 mL), $NaBH_4$, platinum nanoparticles (2–3 nm), 20 kHz, 60 W, 100 °C | 80 |
| $HAuCl_4$ | Au nanobelts | Aqueous solution, α-D-glucose (or β-cyclodextrin), 40 kHz, 100 W, sonication for 10–60 min | 81 |
| $AgNO_3$, $HAuCl_4$ | Ag nanoplates, Au nanorings | PVP, DMF solution (40 mL), ambient conditions, 20 kHz, 60 W $cm^{-2}$, sonication for 0.5 h | 82 |
| $HAuCl_4$ | Au nanocones | 2-Ethoxyaniline, hexane, aqueous solution, 35 kHz, 144 W, 45 °C, sonication for 90 min | 83 |
| $NaAuCl_4$, $PdCl_2$ | Core–shell Au/Pd bimetallic nanoparticles | Aqueous solution (60 mL), sodium dodecyl sulfate, 200 kHz, 200 W, 20 °C | 84 |
| $HAuCl_4$, $AgNO_3$ | Core–shell Au–Ag bimetallic nanoparticles | Aqueous solution (70 mL), polyethylene glycol, ethylene glycol, pH 3.5, argon atmosphere, 20 kHz, 23–47 W $cm^{-3}$, room temperature, sonication for 30 min | 85 |
| $H_2PtCl_6$, $HAuCl_4$ | Au–Pt bimetallic nanoparticles | Aqueous solution (6.0 mL), ascorbic acid solution (6.0 mL), sonication for 15 min | 86 |
| $PtBr_4$, $CuBr_2$ | $PtCu_3$ bimetallic nanoparticles | Tetrahydrofuran (200 mL), 2-propanol (20 mL), lithium metal cuttings, naphthalene, 20 kHz, 15 W $cm^{-2}$, −20 °C, sonication for 90 min | 87 |
| $Pd(NO_3)_2$, $AgNO_3$ | PdAg nanoparticles | Ethylene glycol/water mixture (60 mL), vulcan carbon XC-72, $N_2$ atmosphere, 20 kHz, sonication for 3 h (20 s/20 s, on/off) | 88 |
| $Pd(acac)_2$, $Ni(acac)_2$, $Co(acac)_2$, $Fe(acac)_3$, $Mn(acac)_2$ | PdNi, PdCo, PdFe, PdMn nanoparticles | Ethylene glycol (30 mL), pure Ar, 20 kHz, 150 W, room temperature, sonication for 3 h | 89 |
| $AuCl_3$ | Au nanoclusters | Toluene (4 mL), 30 W, 40 kHz, sonication for 0–180 min | 90 |
| $AgNO_3$ | Ag nanoclusters | PMAA solutions (30 mL), pH 4.5, Ar flow, 20 kHz, 25 W $cm^{-2}$, sonication for 10–180 min | 91 |
| $AgNO_3$ | Ag nanoclusters | Aqueous solution (10 mL), BSA, pH 12, 50 W $cm^{-2}$, 15 °C, sonication for 4 h (7 : 3, ultrasonic time/intermittent time) | 92 |
| $AgNO_3$ | Ag nanoclusters | Aqueous solution (25 mL), glutathione, pH 5.0, 40 KHz, 60 W, sonication for 0–170 s | 93 |
| $Cu(NO_3)_2$ | Cu nanoclusters | Reduced glutathione, $Cu(NO_3)_2$, deionized water (5 mL), pH 6.0, sonication for 15 min | 94 |

materials as well, because its synthesis mechanism is mainly on the basis that the sonolysis of solvent vapor is capable of producing some active reactants without additional reducing agents,[77] for example, H˙ and ˙OH radicals for water, R˙ radicals for volatile organic vapor, and so on. These radicals are able to act as reactants for some redox chemistry in the production of nanostructured materials. Similar to the volatile organometallic compounds, a few nonvolatile metal precursors dissolved in

a volatile solvent can be used to prepare nanostructured metals through ultrasound irradiation, whereas the generated nanometals are usually crystallized well and are not so amorphous as the nanoparticles form volatile precursors. Table 2 summarizes the secondary sonosynthesis of nanostructured metals from the nonvolatile precursors.

For the production of nanostructured noble metals, the sonochemical reduction provides an alternative to traditional approaches such as photochemical reduction, controlled chemical reduction, radiolytic reduction, and solvothermal synthesis. A systematic study on the sonochemical synthesis of spherical Au nanoparticles referred to the finding published by Grieser and co-workers:[78] when $HAuCl_4$ aqueous solution was sonicated in the presence of alcohols or other similar organic additives, Au nanospheres would be formed with Au(III) being reduced to Au(0), and the particle size was not only largely determined by the solvent/surfactant properties but also related to ultrasound frequency. From the point of view of morphology, nonspherical Au nanoparticles have been also prepared by sonochemical reduction. Au(III) could form Au(0) nanorods in the presence of cetyltrimethylammonium bromide and $AgNO_3$,[79] and alternatively, it would lead to the formation of monodispersed Au(0) nano-decahedra when poly(-vinylpyrrolidone) (PVP) is used as a stabilizing polymer.[80] Similarly, Au nanobelts, Au nanocones, Ag nanoplates, Ag nanowires, Ag nanorings, and even bimetallic nanoparticles with a core–shell structure (*e.g.*, Au/Ag, Au/Pt, Au/Pd, and Pt/Ru) have been produced as well by an ultrasound-assisted Ostwald ripening process.[81–89] Significantly, high-intensity ultrasound irradiation was able to extremely create small Au nanoclusters, Ag nanoclusters, and Cu nanoclusters (less than 2 nm) by using some polymer molecules (*e.g.*, polymethylacrylic acid) as a capping agent,[90–94] and such nanoclusters were likely to develop widespread applications in bioimaging, biosensing, and single-molecule studies.

Sonochemical reduction is not limited to the synthesis of nanostructured noble metals, and various metal oxides, metal hydroxides, metal chalcogenides as well as other metal compounds have been also prepared through the treatment of relevant precursors in an analogous manner. For the metal compounds, a typical synthesis way involves the sonication of a solution containing metal salts in the presence of different nonmetal sources, such as air for oxygen, thiourea for sulphur, selenourea for selenium, or others. Kipcak *et al.* carried out sonochemistry-assisted synthesis of magnesium borate where magnesium chloride hexahydrate and different boron sources (borax, tincalconite, boric acid, and boron oxide) were used as the precursor materials.[95] The synthesis yields were higher than 80%, and the outcomes were $MgO(B_2O_3)_3 \cdot 7H_2O$ with high crystallinity as per XRD analyses. Pinkas *et al.* obtained insoluble amorphous uranium phosphates from $UO_2^{2+}$ precursors in high-boiling trialkyl phosphate solutions by sonication.[96] Sonolysis experiments were carried out in a frequency of 20 kHz and a power of 0.49 W $cm^{-3}$ under an argon flow at 40 °C, in which trialkyl phosphates served as a phosphate source creating phosphate species by the decomposition of ester molecules and then reacted with uranium precursors. The efficiency of uranium removal from the solution by sonochemical precipitation was higher than 30%, and the obtained amorphous uranium precipitates could change into crystalline uranium diphosphate ($UP_2O_7$) when heated to 1000 °C. Hence, for the uranium-containing waste streams, sonication might potentially serve as a remote separation for uranium. As an effective light-absorbing material for thin film solar cells, $Cu(In_xGa_{1-x})Se_2$ showed high conversion efficiency, but the traditional synthesis of $Cu(In_xGa_{1-x})Se_2$ compounds involved typically some toxic organic solvents such as hydrazine, ethylenediamine, and polyetheramine, as well as a high reaction temperature. Recently, Park *et al.* designed a substantially greener procedure to yield $Cu(In_{0.7}Ga_{0.3})Se_2$ nanoparticles using a slightly modified sonochemical method,[97] where the reaction was carried out at room temperature with ethanol as the only solvent, $NaBH_4$ as a reducing agent, and 5 hour ultrasound irradiation. The proposed reaction scheme revealed the role of ultrasound irradiation in decomposing the intermediate $Cu_2Se$ in the reaction pathways, so the sonification time was investigated to form the $Cu(In_xGa_{1-x})Se_2$ compounds with the expected crystalline structure. The short-period sonification irradiation was not enough to form the expected crystal structure, and even the signs of $Cu_2Se$ also appeared. Prolonging the sonification time resulted in much better crystallinity, where 5 hour ultrasound irradiation would yield single-phase tetragonal $Cu(In_{0.7}Ga_{0.3})Se_2$ nanocrystals without any $Cu_2Se$ crystals.

Additionally, secondary sonosynthesis provides a feasible, facial and short-time approach for the synthesis of hybrid inorganic materials. By sonicating sodium chloride, silver nitrate and poly(vinyl pyrrolidone) in ethylene glycol, Ag/AgCl nanocubes with a 115 nm edge length have been produced with silver nanoparticles embedded into AgCl cubic matrices.[98] In the formation of hierarchically structured ZnO/CdS microspheres,[99] CdS nanoparticles were produced by the sonication of a cadmium chloride and aqueous thiourea solution accompanied by the hydrothermal formation of ZnO microspheres. Chen *et al.* designed a straightforward approach to synthesize $Cd(OH)_2$/Ag nanorods with a core/satellite structure on the basis of the sonochemical method:[100] cadmium chloride would form $Cd(OH)_2$ nanorods *via* a single sonochemical reaction in a base medium (Fig. 8), followed by the thermal annealing process to obtain highly crystalline CdO nanorods; In the presence of $AgNO_3$ and ammonia, the prepared CdO nanorods would undergo a second ultrasonication to obtain a core/satellite complex. This proposal was feasible, and the $Cd(OH)_2$/Ag core/satellite nanorods were prepared successfully, where the deposition of Ag nanodots was completed on the surface when the cubic CdO transformed into monoclinic crystalline $Cd(OH)_2$. Moreover for the direct surface functionalization of $Cd(OH)_2$ nanorods with Ag nanodots, the microjets, shock waves and turbulent flows generating the cavitation collapse were found to play a crucial role.

The assistance of other technologies can improve the performance of secondary sonosynthesis in materials preparation. In order to decrease the sintering temperature to prepare strontium hexaferrite nanoparticles, Jesús and Miró reported the synthesis of strontium hexagonal ferrite ($SrFe_{12}O_{19}$) by

 

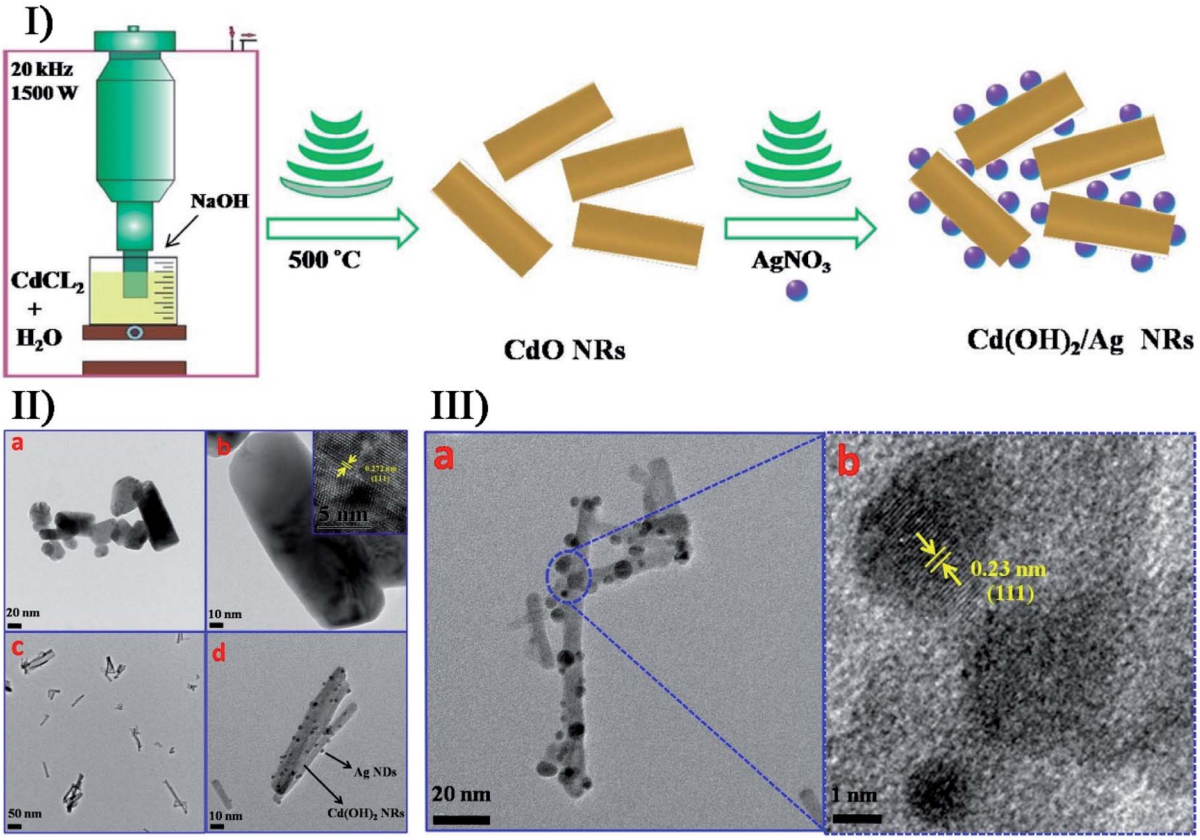


Fig. 8 (I) schematic overview the general mechanism and main steps for the synthesis of CdO and $Cd(OH)_2$/Ag core/satellite nanorods. (II) TEM images of (a, b) CdO nanorods and (c, d) $Cd(OH)_2$/Ag nanorods, where the inset shows the HRTEM image of CdO nanorods in Image b. (III) TEM (a) and HRTEM (b) images of $Cd(OH)_2$/Ag nanorods. Reproduced with permission.[100] Copyright 2018 Elsevier.

sonochemistry and annealing.[101,102] In the synthesis, the sonochemical process yielded an amorphous phase containing $Fe^{3+}$, $Fe^{2+}$ and $Sr^{2+}$ ions from a complexed polyol solution of metallic acetates and diethylene glycol, where $Fe^{2+}$ was partially oxidized to $Fe^{3+}$ due to the formation of $H_2O_2$. Subsequently, annealing of the amorphous phase was carried out at temperatures from 300 to 900 °C providing the intermediate maghemite ($\gamma$-$Fe_2O_3$) at 300 °C, the phase conversion of maghemite to hematite ($\alpha$-$Fe_2O_3$) at 500 °C, and the generation of final $SrFe_{12}O_{19}$ at 800 °C. High sonication output power and long sonication time (up to 3 h) promoted the crystallinity of amorphous phases, decrease in crystal size, and modification of the morphology of particles. Furthermore, the obtained $SrFe_{12}O_{19}$ showed a magnetization of >60 emu $g^{-1}$ consistent with pure hexaferrite obtained by other methods. Similarly, Cavalcante *et al.* synthesized tungstate ($CuWO_4$) crystals with a triclinic structure based on the sonochemical method and the following heating treatment in a conventional furnace.[103] Copper tungstate hydrate precipitated by the sonochemical reaction would remove the partial water molecules in its lattice as treated at a low temperature from 100 °C to 200 °C, and copper tungstate dihydrate ($CuWO_4 \cdot 2H_2O$) would appear at 300 °C, until the crystals were completely occupied by a single $CuWO_4$ triclinic structure at above 400 °C (Fig. 9). Recently, the simultaneous action of ultrasound and hydrothermal treatment, namely sonohydrothermal treatment, has been developed to accelerate crystallization and improve the catalytic performance of nanocrystalline metal oxides. For the first time, Nikitenko *et al.* reported the sonohydrothermal synthesis of nanostructured $(Ce,Zr)O_2$ mixed oxides, and the obtained nanocrystal had a higher external mesoporous surface area than that prepared by ultrasonically assisted coprecipitation followed by hydrothermal treatment.[104] Later, they synthesized stable Ti@$TiO_2$ nanoparticles with a core–shell structure by the sonohydrothermal treatment on air-passivated titanium metal nanoparticles in pure water, in which quasi-spherical Ti particles (20–80 nm) were coated by defect-free anatase crystals (5–15 nm) with small amounts of rutile crystals.[105]

Uzunov *et al.* utilized three synthesis methods (*i.e.*, precipitation; mechanochemical treatment and sonochemistry) to prepare nano-sized zinc oxides from different zinc sources,[106] and the as-synthesized samples had various morphologies with a crystallite size below 20 nm. Under UV irradiation, the sonochemistry-assisted ZnO nanorods exhibited the highest photocatalytic activity for the degradation of malachite green while the precipitation-assisted polycrystalline zinc oxide had a better photocatalytic efficiency under visible irradiation, and on the contrary, the mechanochemistry-assisted nano-sized ZnO led to the deterioration of photocatalytic activity due to inhomogeneous distribution in particles size. In a report of

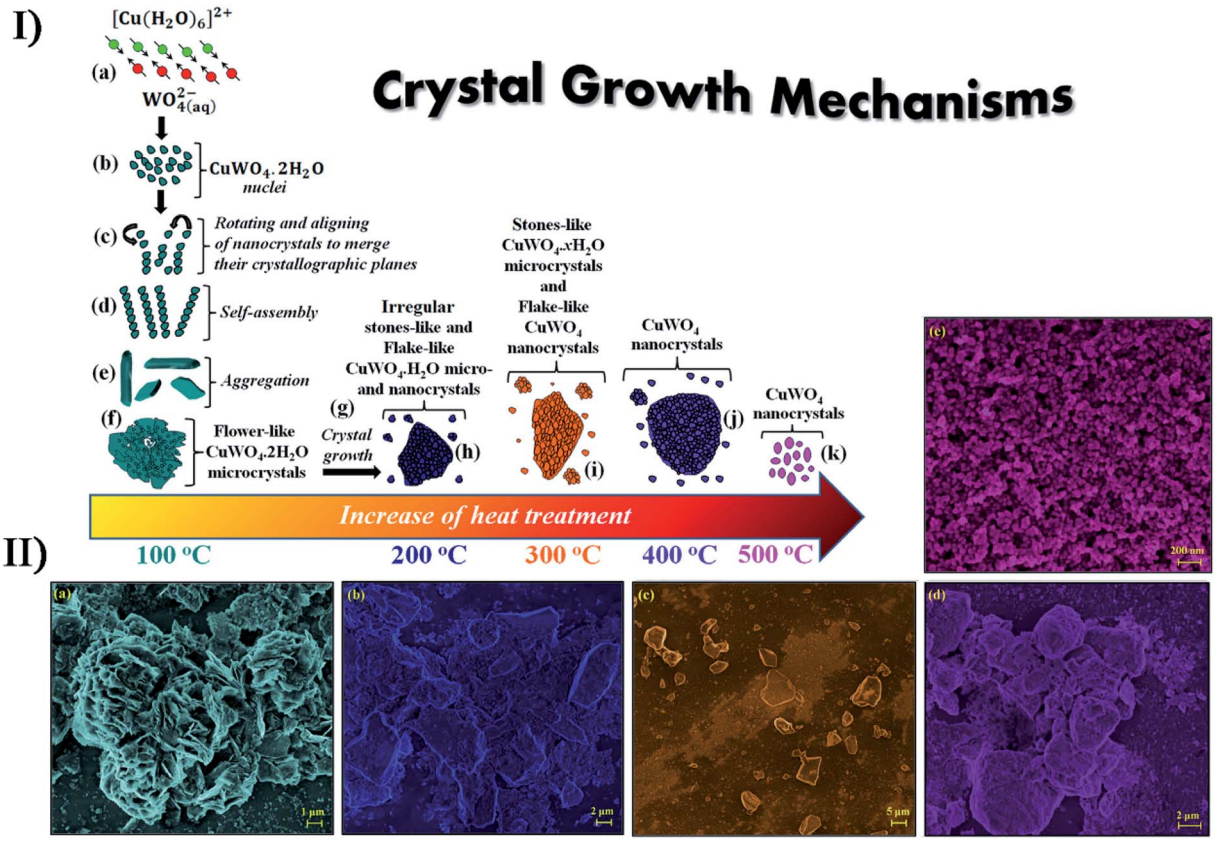


Fig. 9 (I) Schematic representation of the growth mechanism of $CuWO_4 \cdot 2H_2O$ and $CuWO_4$ crystals obtained by the sonochemistry method: (a) reaction between complex ions; (b) appearance of the first $CuWO_4 \cdot 2H_2O$ nuclei; (c) rotation and alignment of nanocrystals, sharing common crystallographic planes; (d) self-assembly process; (e) aggregation of petal-like crystals; (f) formation of flower-like $CuWO_4 \cdot 2H_2O$ microcrystals; (g) crystal growth *via* heat treatment, (h) irregular stone-like $CuWO_4 \cdot 2H_2O$ microcrystals, (i) stone-like $CuWO_4 \cdot 2H_2O$ microcrystals and flake-like $CuWO_4$ nanocrystals; (j) formation of aggregated $CuWO_4$ nanocrystals; (k) crystal growth of flake-like $CuWO_4$ nanocrystals. (II) FE-SEM images of $CuWO_4$ crystals heat treated at different temperatures: (a) 100 °C, (b) 200 °C, (c) 300 °C, (d) 400 °C and (e) 500 °C for 1 h, respectively. Reproduced with permission.[103] Copyright 2017 Elsevier.

Ashiri *et al.*,[107] both the sonochemical processing and the mechanochemical approach were considered for the synthesis of $BaTiO_3$ nanopowders. The contrasting results demonstrated that the sonochemical synthesis could obtain highly pure tetragonal $BaTiO_3$ at a much lower processing temperature and shorter time span because the reactant ions would homogenously order into the perovskite structure in sonication when dissolved in the solution mixture. If there is a proper structure directing agent or template in sonication, more different nanostructured materials can be obtained. Under ammonia conditions, $CdCl_2$ and $NaSeSO_3$ were sonochemically reacted to form hollow CdSe spheres,[108] where $Cd(OH)_2$ from the hydrolysis acted as an *in situ* template. To make ZnO nanorods and nanoflakes, vertically aligned nanostructures could be deposited on the substrates such as Zn sheets, Si wafers and glass by sonicating a zinc salt when hexamethylenetetramine was used as a shape directing agent.[109] In the presence of soft templates, ultrasound can result in the formation of unique morphologies during the synthesis of nanostructured metal oxides. For example, sonicating the $Pb(CH_3COO)_2$, $NaWO_4$ and P123 (a pluronic block copolymer) mixed solution could prepare hollow $PbWO_4$ spindles while only solid particles were obtained in the absence of ultrasound,[110] and the probable reason was that ultrasound changed the P123 micelles into hollow micelle aggregates forming a hollow spindle structure.

## 6. Synergetic sonosynthesis

The synthesis of many materials does not isolate primary sonosynthesis or secondary sonosynthesis, or it goes through the synergy of serial sonosynthesis. Moreover, some physical or mechanical effects from ultrasound irradiation, such as high-speed microjets, intense shock waves, and interparticle collisions, have been frequently applied in preparing emulsions, agglomerating malleable materials, modifying solid surfaces, exfoliating layered materials, and breaking down friable materials, and they also belong to important factors in the formation of nanostructured materials as well as the enhanced mass transfer and the bulk thermal heating. For instance, ultrasonic spray pyrolysis (USP), sonocrystallization, sonofragmentation as well as other technologies on account of the physical or mechanical effects originating from ultrasound have been utilized to make nanostructured materials. Fig. 10 shows that

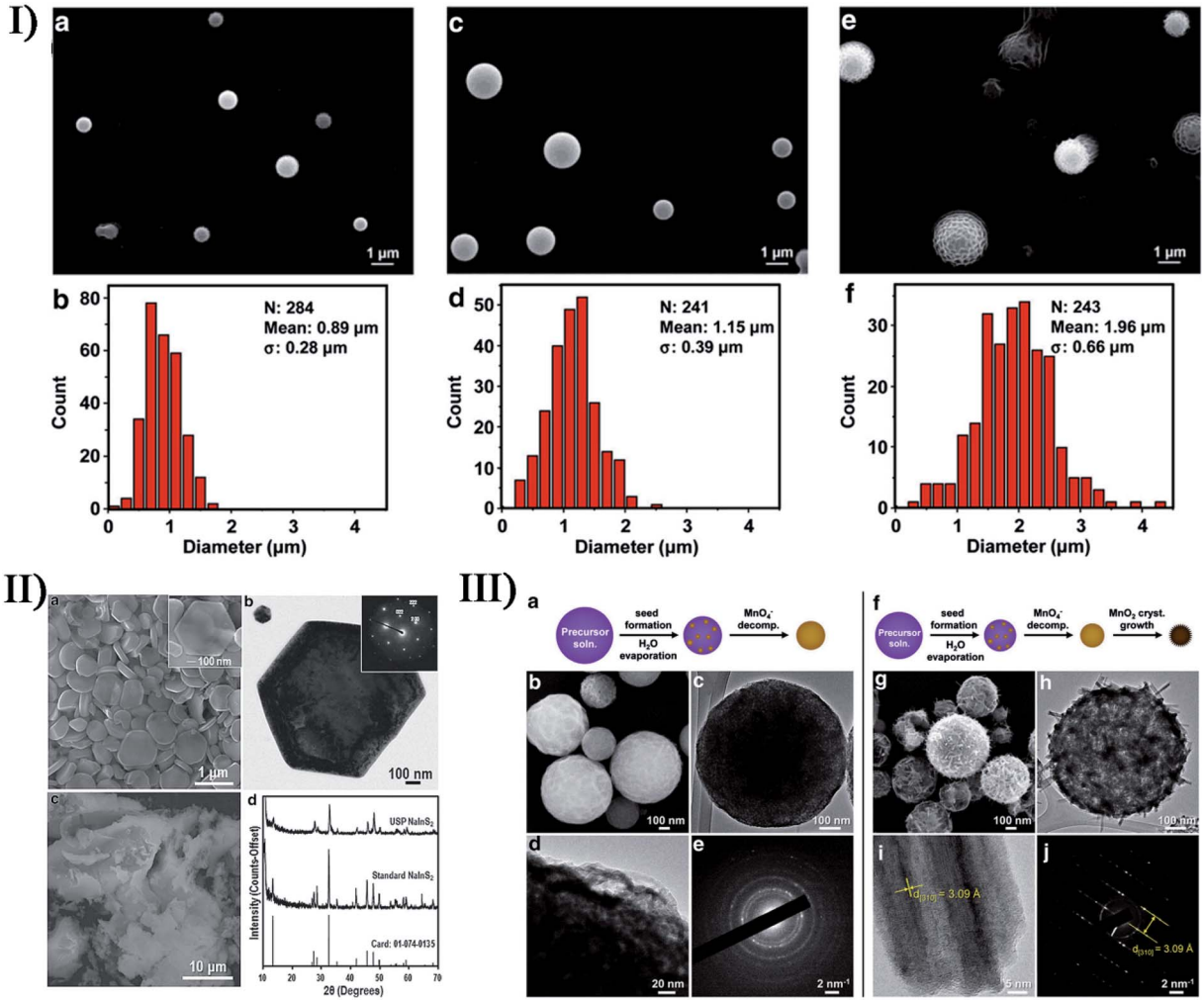


Fig. 10 (I) The SEM images and size distributions of polydimethylsiloxane microspheres prepared using 4 mg $mL^{-1}$ (a, b), 20 mg $mL^{-1}$ (c, d), and 100 mg $mL^{-1}$ (e, f) polydimethylsiloxane in hexanes, respectively. Reproduced with permission.[111] Copyright 2015 Wiley-VCH. (II) SEM (a) and TEM (b) images showing the hexagonal shape of the $NaInS_2$ nanoplates produced *via* USP (the inset electron diffraction pattern in (b) demonstrates the single-crystalline nature), SEM image (c) of $NaInS_2$ prepared through a non-USP method for comparison, and X-ray diffraction patterns (d) of the USP and non-USP materials. Reproduced with permission.[112] Copyright 2012 Wiley-VCH. (III) Morphology of $MnO_2$ microspheres produced *via* USP varies at 150 °C (a–e) and 500 °C (f–j): TEM images (c, d, h, i) where increasing the reaction temperature caused the formation of larger crystals; SEM images (b, g); electron diffraction patterns (e, j). Reproduced with permission.[113] Copyright 2015 Wiley-VCH.

USP creates some nano- and micromaterials.[111–113] As a result, the physical or mechanical effects and the sonochemical effects can play a combined part in many synthesis processes as well, and the notable examples will be described in the latter section.

Ultrasound irradiation has become a broadly useful tool to prepare single and few layered materials by overcoming the attractive forces between individual layers to break 3D layer structures down to 2D planar structures. Hammer's method, as a typical synthesis route to graphene oxide (GO), is often used to oxidize pristine graphite to form graphite oxide, where an increased interlayer distance can consequently weaken the van der Waals force relative to graphite[114] and then produce single or few layered GO by a bath or horn sonication (Table 3).[115–130] The direct exfoliation of graphite by sonication in a suitable solvent (*e.g.* *N*-methyl-pyrrolidone) is a more straightforward method for the formation of single and few layered graphene, in which the surface energy between the solvent and graphite had to match (about 40 mJ $m^{-2}$) to obtain high-yield exfoliated graphene.[131] Other layered materials such as $MoSe_2$, $MoS_2$, $WS_2$ and $Bi_2Te_3$ can also be used to prepare single-layered nanosheets by direct liquid-phase exfoliation under sonication.[132] In some studies, the physical or mechanical effects of ultrasound dramatically enhance the intercalation of guest substances into layered materials along with the sonochemical synthesis. $H_2PtCl_6$ exposure to an $H_2$ gas stream could be ultrasonically applied in graphite layers to prepare Pt-intercalated graphite.[133] K-Intercalated compounds ($KC_8$) also could be prepared by sonicating graphite with potassium in toluene,[134] whereas ultrasonicattion of potassium-intercalated graphite would generate carbon nanoscrolls in ethanol.[135] So far, the detailed reason has been not fully understood. In addition, a few efforts have been paid to deposit the sonochemically produced

Table 3 Sonocatalysis synthesis or exfoliation of graphene derivatives

| Product | Ultrasound | Ref. |
|---|---|---|
| Graphene nanoribbons | 1500 W, 20 kHz | 115 |
| Graphene nanosheets | 500 W | 116 |
| Graphene nanosheets | 20 kHz, 750 W | 117 |
| Graphene nanosheets | — | 118 |
| Graphene dispersions | 51–52 W | 119 |
| Graphene oxide | 600 W | 120 |
| Graphene oxide | 40 kHz, 157 W | 121 |
| Graphite oxide | 360 W | 122 |
| Graphene oxide nanosheets | — | 123 |
| Reduced graphene oxide | 20 kHz, 400 W | 124 |
| Reduced graphene oxide | — | 125 |
| Reduced graphene oxide nanodispersion | 20 kHz, 1000 W or 750 W (ultrasound horn); 130–35 kHz, 200 W (ultrasonic bath) | 126 |
| Sulfonated graphene | 40 W | 127 |
| Sulfonated reduced graphene oxide | 37 kHz | 128 |
| Isocyanate-treated graphene oxide nanoplatelets | 150 W | 129 |
| Chitosan-modified nanoscale graphene oxide | >360 W | 130 |

nanoparticles onto the graphene substrate with a high surface area. Guo *et al.* prepared the $TiO_2$ nanoparticles deposited on graphene sheets by ultrasonically irradiating GO and $TiCl_4$ in ethanol.[136] Au and $Fe_3O_4$ nanoparticles also could be used to couple the GO or the graphene.[137,138]

In addition, ultrasound is a popular method to synthesize other carbon nanomaterials. In traditional carbon nanotube synthesis, sonochemical effects are frequently used to disperse individual single-walled carbon nanotubes in the solution such as *N*-methyl pyrrolidone.[139] In the cases that volatile organometallic precursors were sonicated to form different structured materials as described above,[74,75] *p*-xylene acting as a carbon source in the presence of low-concentration ferrocene could produce single-walled carbon nanotubes on the silica powder under ultrasound irradiation. Recently, Ha and Jeong have reported a similar sonochemical method to prepare multi-walled carbon nanotubes, which required a higher amount of ferrocene and a little water added to the reactant suspension.[140] Carbon nanodots with an average diameter of 2–9 nm were made from the sonication of poly(ethylene glycol)-400 (PEG-400) as a carbon source in a water/silicone oil bath[141,142] and when excited at a 390 nm excitation wavelength, the product had 474 nm emission wavelength and 774 A.U. fluorescence intensity. Based on this, Gedanken *et al.* fabricated an antibacterial material, Ga-doped C-dots on Ga nanoparticles (Ga@C-dots@Ga NPs), where a one-step sonochemical process was applied for the simultaneous fabrication and coating of Ga@C-dots@Ga NPs using PEG-400 and molten gallium (Fig. 11).[143] At present, carbon nanodots have been also sonochemically prepared by using other carbon sources like polyacrylic acid, glucose and citric acid.

The combined effects of sonochemical and physical or mechanical processes can promote the preparation of porous materials as an alternative in some cases. Jung and co-workers used 1-methyl-2-pyrrolidone as a solvent to prepare MOF-177 (MOF or metal–organic framework) or $Zn_4O(BTB)_2$ (BTB or 4,4′,4″-benzene-1,3,5-triyl-tribenzoate), within only an hour by the ultrasound-assisted method.[144] Similarly, the sonochemical preparation of spherical Mg-MOF-74,[145] namely $Mg_2$(DHTP)$(H_2O)_2\cdot 8H_2O$ (DHTP or 2,5-dihydroxyterephthalate), was adapted from the conventional solvothermal method if triethylamine was added to encourage the deprotonation of DHTP. Morsali *et al.* synthesized a nano-structured Cu(II) MOF (namely $\{Cu(BDT)(DMF)\cdot CH_3OH\cdot 0.25DMF\}_n$) by reacting $H_2BDT$ with $Cu(NO_3)_2\cdot 6H_2O$ under ultrasound irradiation,[146] in which $BDT^{2-}$ was 1,4-benzeneditetrazolate and DMF was *N*,*N*-dimethylformamide, wherein the morphology of the MOF could be altered by ultrasound irradiation at different temperatures, *e.g.*, yielding rice grain-like, pellet-like and laminate-like structures at 10, 40 and 70 °C. In another study, they used such synergetic sonochemical synthesis to prepare a pillared-layer Zn(II)-based MOF,[147] namely $[Zn_2(NH_2\text{-}BDC)_2(4\text{-}bpdh)]\cdot 3DMF$ (TMU-16-$NH_2$), where $NH_2$-BDC was amino-1,4-benzenedicarboxylate and 4-bpdh was 2,5-bis(4-pyridyl)-3,4-diaza-2,4-hexadiene. By the comparison, they found that the sonication time, sonication power and initial reagent concentrations had an important effect on the morphology of TMU-16-$NH_2$, for example, longer sonication time, lower initial reagent concentrations, and higher sonication power could lead to uniform nanocubes. Later, they synthesized a dihydro-tetrazine functionalized MOF *via* ultrasonic and reflux methods,[148] where $[Zn(OBA)(H_2\text{-}DPT)_{0.5}]\cdot DMF$ (TMU-34) was prepared using 4,4′-oxybis(benzoic acid)($H_2$OBA) as a dicarboxylate oxygen donor ligand and 3,6-di(pyridin-4-yl)-1,4-dihydro-1,2,4,5-tetrazine ($H_2$DPT) as a pillar spacer. In this synthesis, increasing the sonication time could reduce aggregation morphology, decreasing the initial reagent concentrations could form a uniform plate-like morphology, and enhancing the sonication power could obtain a separate uniform plate-like morphology with a thickness of about 100 nm. The obtained TMU-34 showed a noticeable response to Al(III) ions; moreover, the nano-sized sample with a uniform separated plate-like morphology had a higher detection limit and speed due to the fast diffusion of Al(III) inside the framework as well as close contact and strong interaction of Al(III) with the dihydro-tetrazine group. Additionally, other porous materials such as MOF-5, IRMOF-3 or manganese dioxide octahedral molecular sieves have been also produced by ultrasonic methods.[149–151]

In the preparation of porous nanostructures under ultrasound irradiation, the combined effects can be also utilized to alter the size and distribution of nanomaterials. The ZIF-8 nanoparticles (ZIF or zeolitic imidazolate framework) with an around 200 nm diameter were prepared through the precipitation of zinc nitrate and 2-methylimidazole mixed in methanol,[152] where a bimodal distribution would be caused as an evidence of Ostwald ripening when the nanoparticles were subjected to sonication. Through the sonosynthesis techniques, Kim *et al.* developed a rapid and facile method for the *in situ* growth of MOF films over a metal substrate,[153] in which high-intensity ultrasound enhanced the reactivity between metal

 

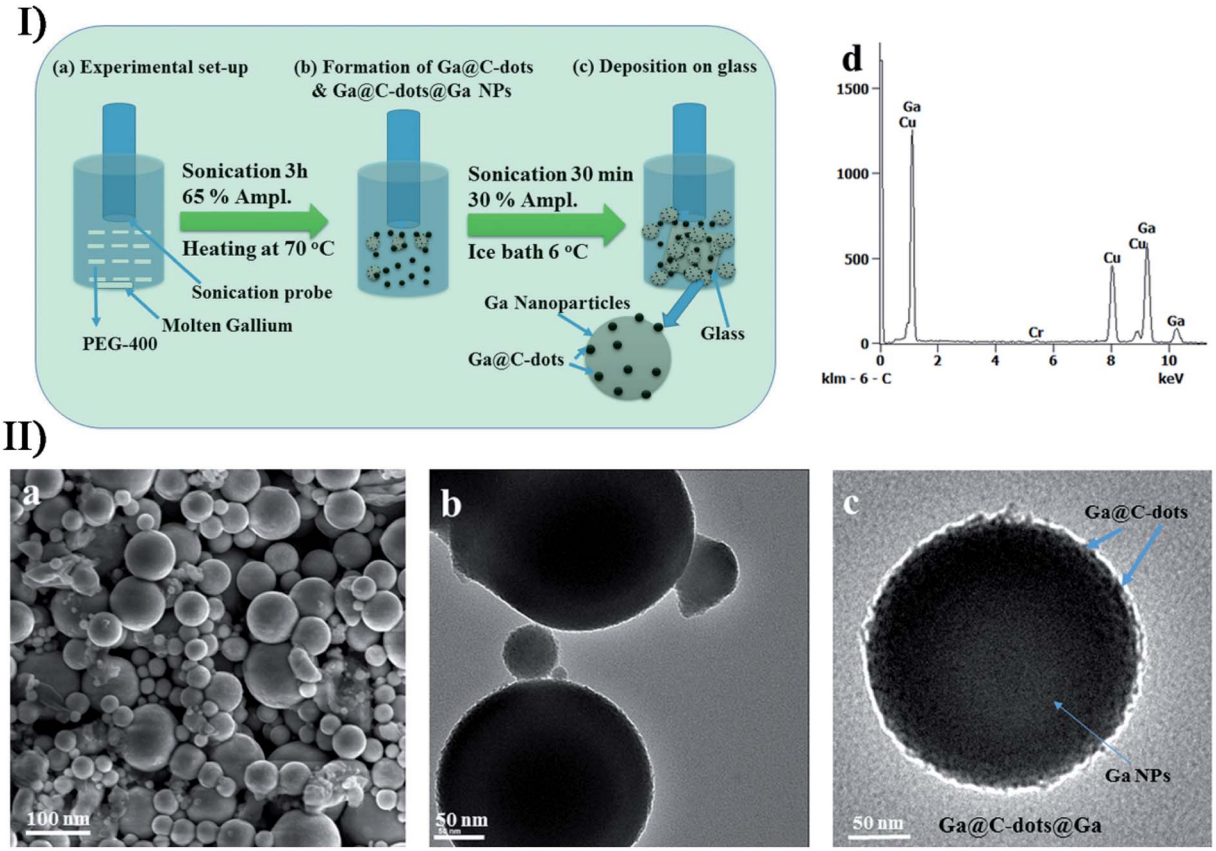


Fig. 11 (I) Schematic overview of the sonochemical deposition process for self-assembly of Ga@C-dots and Ga@C-dots@Ga NPs: (a) sonication set-up, (b) formation of Ga@C-dots/Ga@C-dots@Ga NPs, and (c) Ga@C-dots and Ga@C-dots@Ga NPs decorated on a glass substrate. (II) (a) SEM micrograph, (b) TEM images, (c) magnified view of single particles and (d) EDS spectrum of Ga@C-dots@Ga NPs. Reproduced with permission.[143] Copyright 2017 Royal Society of Chemistry.

ion sources and organic ligands after the metal substrate was first treated oxidatively to produce the corresponding metal hydroxide. On the Cu or Zn metal substrates, researchers used such an approach to successfully fabricate four MOF films including Cu-BDC film, Cu-BTC film, ZIF-8 film and MOF-5 film, and found that the crystal size in the films increased with the sonication time except for the MOF-5 film (Fig. 12). On the contrary, MOF-5 had a decrease in the crystallization and growth rate when exposed to long-period ultrasound irradiation, which was likely because the complex formation of several nuclei leaded to a decrease in crystal size.

Furthermore, the combined effects of ultrasound can also participate in the sonochemical synthesis and/or modification *via* other approaches, *e.g.*, ultrasound can be applied in promoting the diffusion of dopants into the nanostructured materials. In the study of Xiong *et al.*, high-intensity ultrasound was used to prepare photoluminescence-tunable $Mg^{2+}$ doped ZnO nanoparticles with no MgO phase existing in the ZnO nanoparticles.[154] In the study of Belova *et al.*, ultrasound irradiation was used to make a slurry containing Au colloids and $TiO_2$ particles to produce an Au nanoparticle-intercalated mesoporous $TiO_2$ structure which had enhanced photocatalytic properties.[155] Recently, Wickleder *et al.* described a novel ionic liquid-assisted synthesis strategy to produce $Eu^{2+}$-doped BaFCl nanoparticles by applying sonochemical approaches,[156] where 1-butyl-3-methylimidazolium tetrafluoroborate (BmimBF4) was used as the fluoride source with $EuBr_2$ or $EuSO_4$ as the europium source. $Eu^{2+}$-doped BaFCl nanoparticles were stably suspended in BminBF4 presenting a relatively narrow size distribution between 20 and 90 nm, where 80% of the particles were smaller than 40 nm (Fig. 13I). Under daylight, the suspensions with undoped and doped barium fluoride chloride nanoparticles were both colorless because a high reflectance value (above 97%) in the visible range caused nearly no efficient absorbance. The reflectance decreases in the UV spectral range, allowing the undoped BaFCl particles to display weak dark blue emission probably originating from the C-dot present in the ionic liquid while $Eu^{2+}$-doped BaFCl particles emitted efficient bluish white light (Fig. 13II). By such a combination of ionic liquid and sonication, $Eu^{3+}$-doped lanthanide nanophosphates were also fabricated from $Ln(NO_3)_3 \cdot 6H_2O$ and 1-hexyl-3-methylimidazolium dihydric phosphate. Nagabhushana *et al.* reported the synthesis of $Eu^{3+}$-doped $Y_2O_3$ nanophosphors by a modified sonochemical method using aloe vera gel as a surfactant[157] and investigated the effect of sonication time on the morphology of nanophosphors. Within a short sonication time, the nanophosphors showed agglomerated microstructures, and with the sonication time increasing, the size slightly

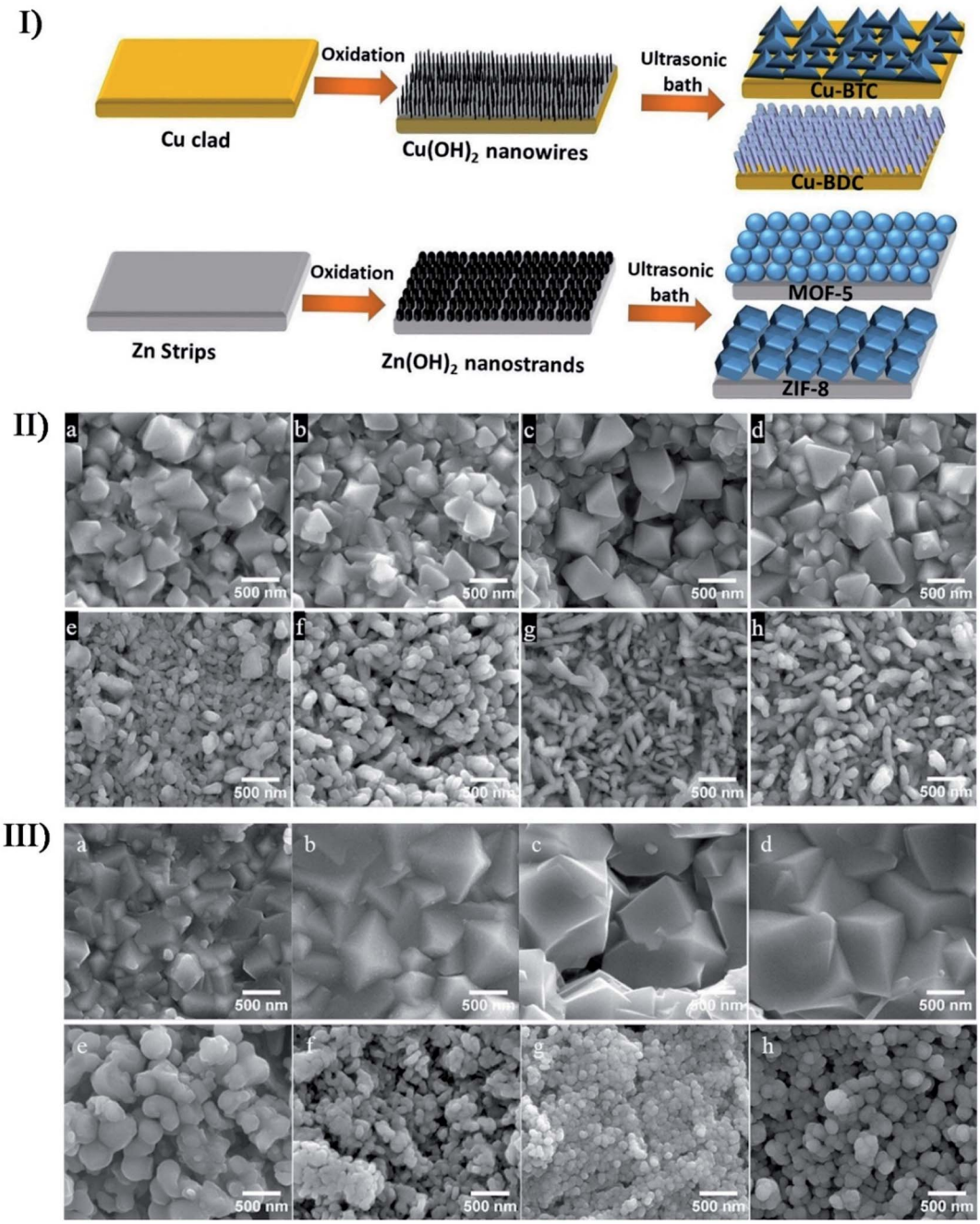


Fig. 12 (I) Schematic illustration of the two-step method for the fabrication of different thin MOF films. (II) SEM images of Cu-BTC with 0.5 mM BTC under ultrasonic irradiation for (a) 5 min, (b) 15 min, (c) 30 min, and (d) 60 min; SEM images of Cu-BDC with 1 mM BDC under ultrasonic irradiation for (e) 5 min, (f) 15 min, (g) 30 min, and (h) 60 min. (III) SEM images of ZIF-8 with 0.1 mM 2-MIM under ultrasonic irradiation for (a) 5 min, (b) 15 min, (c) 30 min, and (d) 60 min. SEM images of MOF-5 with 1 mM BDC under ultrasonic irradiation for (e) 5 min, (f) 15 min, (g) 30 min, and (h) 60 min. Reproduced with permission.[153] Copyright 2018 Elsevier.

reduced and began to be uniformly spherical until a prolonged sonication time of over 6 hours caused agglomerated microstructures again because uniform spherical structures were thriving themselves. Previous to Wickleder *et al.* and Nagabhushana *et al.*, Xu and co-workers had successfully synthesized hexagonal and tetragonal $LnPO_4$:$Eu^{3+}$ nanostructures (Ln = La, Gd, and Y) through a simple and facile ionic liquid-assisted sonochemical method,[158] where the rapid reaction rate was attributed to the acceleration effect of ionic liquid combined with ultrasound irritation. The obtained $LnPO_4$:$Eu^{3+}$ displayed four different types of morphologies including nanowires, nanorods, nanowire bundles and nanoparticles, which might be relevant to the period of the sonication process.

In addition, what is more, the microjets and shock waves originating from the ultrasound near the solid materials can induce a few physical changes on the surface of particles or

 

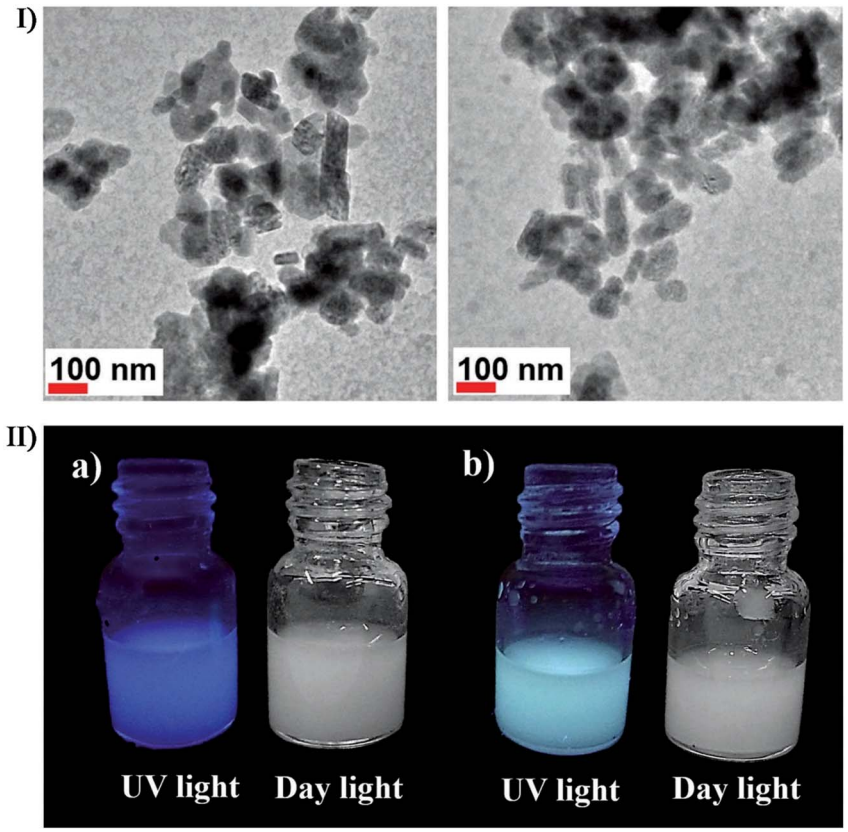


Fig. 13 (I) TEM images of BaFCl:$Eu^{2+}$ nanoparticles which were prepared using EuBr in an ultrasonic bath for 30 min. (II) $Eu^{2+}$-undoped (a) and $Eu^{2+}$-doped (b) BaFCl nanoparticles suspended in $BminBF_4$ under UV and daylight. Reproduced with permission.[156] Copyright 2018 Wiley-VCH.

substrates. For instance, the anticorrosion surface coatings can be improved *via* the treatment of high-intensity ultrasound in which a newly active oxide layer will form with the existing oxide layer being removed. Ultrasound irradiation can also improve the sol–gel preparation of nanostructured metal oxides by accelerating the hydrolysis process, improving the phase purity, and creating the metal oxides with narrower size distribution and higher surface area. In a study of Yu *et al.*, $TiO_2$ nanoparticles produced by the ultrasound irradiation of the precursor solution had a higher photocatalytic activity,[159] which was attributed to the accelerated hydrolysis in sonication improving the crystallinity of $TiO_2$. To obtain thin zirconium dioxide layers on structured reactors, Jodłowski developed an efficient ultrasound-assisted sol–gel method through the synergistic combination of three processes including the sonochemical synthesis of Zr sol–gel from a Zr(IV) *n*-propoxide precursor solution,[160] the addition of ethylene glycol and glycerol as stabilizing agents, and the deposition of $ZrO_2$ on FeCr alloy supports using the dip-coating method. The results displayed that the $ZrO_2$ films on the metallic structure were dense and uniform without any impurities. In the study of Sierra-Salazar *et al.*, the hierarchically porous Pt/$SiO_2$ catalyst was prepared in aqueous medium *via* the combination of latex synthesis, sonochemical reduction and a two-step catalysed sol–gel process, and its mesopore and macropore size ranged as large as 2–15 nm and 90–400 nm, respectively.[161,162] For such a silica-supported Pt catalyst, the noble metal Pt distribution could be enhanced at low loadings by controlling the hierarchical porosity of the support material.[162] Manoharan *et al.* tailored a hybrid method of the precipitation technique and ultrasonication to accomplish the preparation of polycrystalline zirconia nanophosphors from a zirconium oxalate precursor complex.[163] As a physical aid to the synthesis process, the acoustic wave well controlled the grain size of nano-zirconia where the particles had a uniform spherical shape and narrow size distribution in the range of 15–25 nm, and the crystal structure was found to be predominantly tetragonal at room temperature. By the sonochemical coprecipitation, Zhang *et al.* prepared catalase-inorganic hybrid microflowers (Cat-HMFs) by using catalase as an organic component and copper phosphate ($Cu_3(PO_4)_2$) as an inorganic component.[164] Then, Cat-HMFs were dropped onto the glassy carbon electrode to fabricate a $H_2O_2$ biosensor. Amperometric detection results indicated that such a biosensor displayed excellent current response stability, selectivity and long-term storage stability toward $H_2O_2$ detection.

Certainly, the inorganic-based hybrid nanomaterials such as inorganic/polymer composites and inorganic/biomolecule composites or other multi-level composites have been produced largely based on combined sonosynthesis. For instance, Ashokkumar *et al.* carried out the sonochemical formation of polystyrene/$SiO_2$ Janus particles on the basis of the

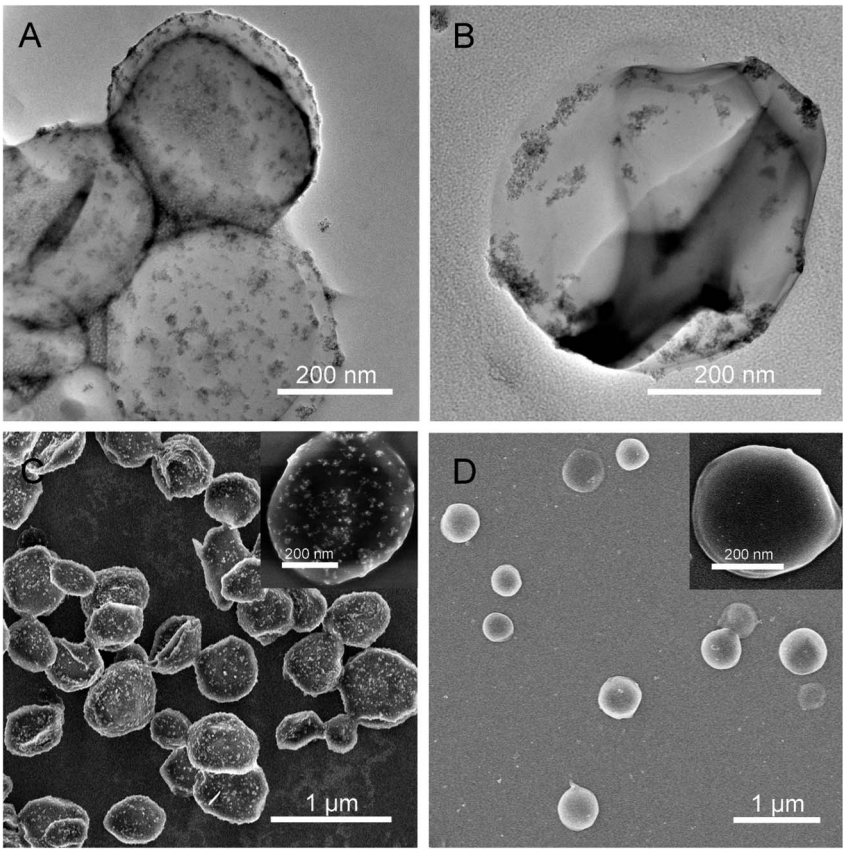


Fig. 14 TEM images of organic/BSA composites with a magnetic shell (A) and with a magnetic core (B); SEM images of organic/BSA composites with a magnetic shell (C) and with a magnetic core (D), where the close-up images lay in the inset of panel (C) and (D). Reproduced with permission.[166] Copyright 2019 Elsevier.

phase separation mechanism between the tetraethoxysilane and growing polystyrene particles.[165] In our studies, the magnetic nanoparticles were either fixed on the surface of carrier supporters as a shell or loaded into the interior of carrier supporters as a core (Fig. 14).[166] We have been also reviewed the sonochemical fabrication of inorganic/biomolecule composites for drug delivery and described the multiformity and multifunctionality of products according to the synthetic materials, implementation schemes, or specific demands. In fact, the structure, size, stability and activity of inorganic-based hybrid nanomaterials are important to both the quality of properties and the acceptability of applications, and the relevant research results or viewpoints have been reviewed in detail in other papers.[167–173]

## 7. Future outlook

Ultrasound-aided materials synthesis has been developed rapidly and remarkably in the last few decades, constantly in a few novel ways to simplify the synthesis processes or to enhance the properties of products. Indeed, ultrasound irradiation shows potential to assemble nano-structured inorganic materials of defined sizes and with pre-defined functionalities, or together with the recent advances or methods for purpose-specific or site-specific modification, significantly expands its applications in materials synthesis. Thereby, nano-structured inorganic materials in association with sonochemical synthesis are an available future direction. Even so, many challenges and anticipations are still online for the in-depth development of either sonosynthesis or the resultant products. The probable challenges could be as follows: more mechanistic and experimental understanding of the cavitation phenomenon on the nano- and micro-levels is needed to settle a matter in controlling the sonosynthesis processes; the difference of raw materials or a variety of microdevices asks for more designs of ultrasound-based synthesis platforms; sometimes for the ultrasound-assisted preparation of nanostructured materials, controlled morphologies, structures, and compositions are essential but a lot unsolved; the performance, durability, selectivity as well as low cost of product materials are still highly demanding; besides a high mechanical stability and a long shelf life, all the products had to accurately act according to on-site conditions or stimulus; finally, sonosynthesis is an energy consuming process in materials preparation, and although the production of ultrasound from electrical power can be extremely efficient, sonochemistry remains energy inefficient since the coupling of ultrasound into chemically useful cavitation events has low yield, so more effective ways to induce more cavitation in liquids may alleviate the current limitation. Certainly, there are more known and unknown areas meriting

 

further study on ultrasound or sonochemical synthesis, such as the interaction mechanism between the materials at the cavitation interface, the controlled energy distribution of collapsing bubbles, the heterogeneous nucleation onto the solid surfaces with different properties, the *in situ* observation of the product's macroscopic structures in the formation, and so on.

## 8. Conclusion

Ultrasound is appealing and conducive to the preparation or modification of nanomaterials. This review simply gives the view on the chemical, physical and mechanical effects from ultrasound irradiation, presenting the basic principles or mechanisms of primary sonosynthesis and secondary sonosynthesis. Meanwhile, it describes the preparation of inorganic materials from the perspective of sonosynthesis, highly focusing on different inorganics including metals, alloys, metal compounds (*e.g.*, metal oxides, metal sulfides, and metal nitrides), non-metals (*e.g.*, carbon materials, silicon materials, and selenium materials) and hybrid composites, and widely covering a variety of structures such as solid structures, hollow structures, core–shell structures, porous structures, nanotube structures, nanorod structures, and layered structures. In addition, the review also provides the probable challenges and technological potential for the future advancements on the sonochemical synthesis applications. We hope that such a review can provide a comprehensive understanding of sonochemistry as well as the synthesis mechanism and broaden the updated applications in catalysis or other fields.

## Conflicts of interest

There are no conflicts to declare.

## Acknowledgements

The authors would like to thank the Natural Science Foundation of Shandong (ZR2020MB063), the Taishan Scholar Program of Shandong Province (ts201511027), the China Postdoctoral Science Foundation (2017M622125), and the Research Project of Postdoctoral Application in Qingdao. Thanks to the Royal Society of Chemistry, Elsevier, the American Chemical Society, Springer and Wiley-VCH for the copyright permissions of reproduction, adaptation, and redrawing of figures.

## Notes and references

1 G. Chatel, How sonochemistry contributes to green chemistry?, *Ultrason. Sonochem.*, 2018, **40**, 117–122.
2 T. J. Mason, Industrial, sonochemistry: potential and practicality, *Ultrasonics*, 1992, **30**, 192–196.
3 N. Pokhrel, P. K. Vabbina and N. Pala, Sonochemistry: science and engineering, *Ultrason. Sonochem.*, 2016, **29**, 104–128.
4 Z. Li, T. Zhuang, J. Dong, L. Wang, J. Xia, H. Wang, X. Cui and Z. Wang, Sonochemical fabrication of inorganic nanoparticles for applications in catalysis, *Ultrason. Sonochem.*, 2021, **71**, 105384.
5 K. Hanajiri, T. Maruyama, Y. Kaneko, H. Mitsui, S. Watanabe, M. Sata, R. Nagai, T. Kashima, J. Shibahara, M. Omata and Y. Matsumoto, Microbubble-induced increase in ablation of liver tumors by high-intensity focused ultrasound, *Hepatol. Res.*, 2006, **36**, 308–314.
6 S. L. Poliachik, W. L. Chandler, P. D. Mourad, R. J. Ollos and L. A. Crum, Activation, aggregation and adhesion of platelets exposed to high-intensity focused ultrasound, *Ultrasound in Medicine and Biology*, 2001, **27**, 1567–1576.
7 Y. S. Tung, H. L. Liu, C. C. Wu, K. C. Ju, W. S. Chen and W. L. Lin, Contrast-agent-enhanced ultrasound thermal ablation, *Ultrasound in Medicine and Biology*, 2006, **32**, 1103–1110.
8 M. A. Almessiere, A. V. Trukhanov, F. A. Khan, Y. Slimani, N. Tashkandi, V. A. Turchenko, T. I. Zubar, D. I. Tishkevich, S. V. Trukhanov, L. V. Panina and A. Baykal, Correlation between microstructure parameters and anti-cancer activity of the $[Mn_{0.5}Zn_{0.5}](EuxNdxFe_{2-2x})O_4$ nanoferrites produced by modified sol-gel and ultrasonic methods, *Ceram. Int.*, 2020, **46**, 7346–7354.
9 L. Qiu, Y. Jiang, L. Zhang, L. Wang and Y. Luo, Ablation of synovial pannus using microbubble-mediated ultrasonic cavitation in antigen-induced arthritis in rabbits, *Rheumatol. Int.*, 2012, **32**, 3813–3821.
10 K. Yamamoto, P. M. King, X. Wu, T. J. Mason and E. M. Joyce, Effect of ultrasonic frequency and power on the disruption of algal cells, *Ultrason. Sonochem.*, 2015, **24**, 165–171.
11 M. A. Almessiere, Y. Slimani, A. D. Korkmaz, S. Güner, A. Baykal, S. E. Shirsath, I. Ercan and P. Kögerler, Sonochemical synthesis of $Dy^{3+}$ substituted $Mn_{0.5}Zn_{0.5}Fe_{2-x}O_4$ nanoparticles: Structural, magnetic and optical characterizations, *Ultrason. Sonochem.*, 2020, **61**, 104836.
12 S. Anandan, V. K. Ponnusamy and M. Ashokkumar, A review on hybrid techniques for the degradation of organic pollutants in aqueous environment, *Ultrason. Sonochem.*, 2020, **67**, 105130.
13 S. Ye, M. Yan, X. Tan, J. Liang, G. Zeng, H. Wu, B. Song, C. Zhou, Y. Yang and H. Wang, Facile assembled biochar-based nanocomposite with improved graphitization for efficient photocatalytic activity driven by visible light, *Appl. Catal., B*, 2019, **250**, 78–88.
14 M. A. Almessiere, Y. Slimani, A. D. Korkmaz, A. Baykal, H. Albetran, T. A. Saleh, M. Sertkol and I. Ercan, A study on the spectral, microstructural, and magnetic properties of Eu-Nd double-substituted $Ba_{0.5}Sr_{0.5}Fe_{12}O_{19}$ hexaferrites synthesized by an ultrasonic-assisted approach, *Ultrason. Sonochem.*, 2020, **62**, 104847.
15 B. M. Teo, Ultrasonic synthesis of polymer nanoparticles, *Handbook of Ultrasonics and Sonochemistry*, 2015, pp. 1–29.
16 M. A. Almessiere, Y. Slimani, U. Kurtan, S. Guner, M. Sertkol, S. E. Shirsath, S. Akhtar, A. Baykal and I. Ercan, Structural, magnetic, optical properties and cation distribution of nanosized $Co_{0.7}Zn_{0.3}Tm_xFe_{2-x}O_4$

(0.0 < x < 0.04) spinel ferrites synthesized by ultrasonic irradiation, *Ultrason. Sonochem.*, 2019, **58**, 104638.
17 L. H. Thompson and L. K. Doraiswamy, Sonochemistry: science and engineering, *Ind. Eng. Chem. Res.*, 1999, **38**, 1215–1249.
18 M. Bradley, M. Ashokkumar and F. Grieser, Sonochemical production of fluorescent and phosphorescent latex particles, *J. Am. Chem. Soc.*, 2003, **125**, 525–529.
19 M. T. Taghizadeh and T. Asadpour, Effect of molecular weight on the ultrasonic degradation of poly(vinyl-pyrrolidone), *Ultrason. Sonochem.*, 2009, **16**, 280–286.
20 M. A. Almessiere, Y. Slimani, H. Güngüneş, V. G. Kostishyn, S. V. Trukhanov, A. V. Trukhanov and A. Baykal, Impact of $Eu^{3+}$ ion substitution on structural, magnetic and microwave traits of Ni-Cu-Zn spinel ferrites, *Ceram. Int.*, 2020, **46**, 11124–11131.
21 N. K. Morya, P. K. Iyer and V. S. Moholkar, A physical insight into sonochemical emulsion polymerization with cavitation bubble dynamics, *Polymer*, 2008, **49**, 1910–1925.
22 J. Gonzalez-Garcia, V. Saez, I. Tudela, M. I. Diez-Garcia, M. D. Esclapez and O. Louisnard, Sonochemical treatment of water polluted by chlorinated organocompounds. A review, *Water*, 2010, **2**, 28–74.
23 M. Siddique, R. Farooq, Z. M. Khan, Z. Khan and S. Shaukat, Enhanced decomposition of reactive blue 19 dye in ultrasound assisted electrochemical reactor, *Ultrason. Sonochem.*, 2011, **18**, 190–196.
24 B. R. Carvalho and M. A. Pimenta, Resonance Raman spectroscopy in semiconducting transition-metal dichalcogenides: basic properties and perspectives, *2D Mater.*, 2020, **7**, 042001.
25 A. P. Kiseleva, G. O. Kiselev, V. O. Nikolaeva, G. Seisenbaeva, V. Kessler, P. V. Krivoshapkin and E. F. Krivoshapkina, Hybrid spider silk with inorganic nanomaterials, *Nanomaterials*, 2020, **10**, 1853.
26 E. J. Braham, R. D. Davidson, M. Al-Hashimi and R. Arroyave, Navigating the design space of inorganic materials synthesis using statistical methods and machine learning, *Dalton Trans.*, 2020, **49**, 11480–11488.
27 R. Wang, Y. Wei, L. An, R. Yang, L. Guo, Z. Weng, P. Da, W. Chen, J. Jin, J. Li and P. Xi, Construction and application of interfacial inorganic nanostructures, *Chin. J. Chem.*, 2020, **38**, 772–786.
28 D. G. Shchukin and H. Moehwald, Sonochemical nanosynthesis at the engineered interface of a cavitation microbubble, *Phys. Chem. Chem. Phys.*, 2006, **8**, 3496–3506.
29 A. Tinoco, A. Ribeiro, C. Oliveira, P. Parpot, A. Gomes and A. Cavaco-Paulo, Albumin/asparaginase capsules prepared by ultrasound to retain ammonia, *Appl. Microbiol. Biotechnol.*, 2016, **100**, 9499–9508.
30 Z. Li, Z. Wang, X. Du, C. Shi and X. Cui, Sonochemistry-assembled stimuli-responsive polymer microcapsules for drug delivery, *Adv. Healthcare Mater.*, 2018, **7**, 1701326.
31 M. Vinatoru and T. J. Mason, Can sonochemistry take place in the absence of cavitation? – a complementary view of how ultrasound can interact with materials, *Ultrason. Sonochem.*, 2019, **52**, 2–5.
32 T. Leighton, *The Acoustic Bubble*, Academic press, 2012.
33 K. S. Suslick, The chemical effects of ultrasound, *Sci. Am.*, 1989, **260**, 80–86.
34 C. R. Brenner, *Cavitation and Bubble Dynamics*, Oxford University Press, Oxford, 1995.
35 K. S. Suslick, N. C. Eddingsaas, D. J. Flannigan, S. D. Hopkins and H. X. Xu, The chemical history of a bubble, *Acc. Chem. Res.*, 2018, **51**, 2169–2178.
36 T. G. McKenzie, F. Karimi, M. Ashokkumar and P. G. G. Qiao, Ultrasound and sonochemistry for radical polymerization: sound synthesis, *Chem.–Eur. J.*, 2019, **25**, 5372–5388.
37 D. V. Prasad Naidu, R. Rajan, R. Kumar, K. S. Gandhi, V. H. Arakeri and S. Chandrasekaran, Modeling of a batch sonochemical reactor, *Chem. Eng. Sci.*, 1994, **49**, 877–888.
38 M. H. Entezari, P. Kruus and R. Otson, The effect of frequency on sonochemical reactions. III: dissociation of carbon disulfide, *Ultrason. Sonochem.*, 1997, **4**, 49–54.
39 M. A. Margulis, Sonoluminescence and sonochemical reactions in cavitation fields. A review, *Ultrasonics*, 1985, **23**, 157–169.
40 A. A. Ndiaye, R. Pflieger, B. Siboulet and S. I. Nikitenko, The origin of isotope effects in sonoluminescence spectra of heavy and light water, *Angew. Chem., Int. Ed.*, 2013, **52**, 2478–2481.
41 R. Silva, H. Ferreira, N. G. Azoia, U. Shimanovich, G. Freddi, A. Gedanken and A. C. Paulo, Insights on the mechanism of formation of protein microspheres in a biphasic system, *Mol. Pharmaceutics*, 2012, **9**, 3079–3088.
42 R. Ji, R. Pflieger, M. Virot and S. I. Nikitenko, Multibubble sonochemistry and sonoluminescence at 100 kHz: the missing link between low- and high-frequency ultrasound, *J. Phys. Chem. B*, 2018, **122**, 6989–6994.
43 N. S. M. Yusof and M. Ashokkumar, Sonochemical synthesis of gold nanoparticles by using high intensity focused ultrasound, *ChemPhysChem*, 2015, **16**, 775–781.
44 J. J. Hinman and K. S. Suslick, Nanostructured materials synthesis using ultrasound, *Top. Curr. Chem.*, 2017, **375**, 12.
45 K. S. Suslick, Sonochemistry, *Science*, 1990, **247**, 1439–1445.
46 J. R. Blake and D. C. Gibson, Cavitation bubbles near boundaries, *Annu. Rev. Fluid. Mech.*, 1987, **19**, 99–123.
47 C. D. Ohl, T. Kurz, R. Geisler, O. Lindau and W. Lauterborn, Bubble dynamics, shock waves and sonoluminescence, *Philos. Trans. R. Soc., A*, 1999, **357**, 269.
48 D. G. Shchukin, D. Radziuk and H. Moehwald, Ultrasonic fabrication of metallic nanomaterials and nanoalloys, *Annu. Rev. Mater. Res.*, 2010, **40**, 345–362.
49 J. H. Bang and K. S. Suslick, Applications of ultrasound to the synthesis of nanostructured materials, *Adv. Mater.*, 2010, **22**, 1039–1059.
50 M. Guo, K. Li, H. Zhang, X. Min, X. Hu, W. Guo, J. Jia and T. Sun, Enhanced catalytic activity of oxygenated VOC deep oxidation on highly active in-situ generated $GdMn_2O_5/GdMnO_3$ catalysts, *J. Colloid Interface Sci.*, 2020, **578**, 229–241.
51 J. Z. Y. Tan, S. Gavrielides, M. Belekoukia, W. A. Thompson, L. Negahdar, F. Xia, M. M. Maroto-Valer and A. M. Beale,

 

Synthesis of $TiO_{2-x}/W_{18}O_{49}$ hollow double-shell and core-shell microspheres for $CO_2$ photoreduction under visible light, *Chem. Commun.*, 2020, **56**, 12150–12153.

52 Z. Wang, H. Yang, R. Liu, S. Xie, Y. Liu, H. Dai, H. Huang and J. Deng, Probing toluene catalytic removal mechanism over supported Pt nano- and single-atom-catalyst, *J. Hazard. Mater.*, 2020, **392**, 122258.

53 Z. Li, L. Qiang, S. Zhong, H. Wang and X. Cui, Synthesis and characterization of monodisperse magnetic $Fe_3O_4$@BSA core-shell nanoparticles, *Colloids Surf., A*, 2013, **436**, 1145–1151.

54 K. S. Suslick, S. B. Choe, A. A. Cichowlas and M. W. Grinstaff, Sonochemical synthesis of amorphous iron, *Nature*, 1991, **353**, 414–416.

55 M. W. Grinstaff, A. A. Cichowlas, S. B. Choe and K. S. Suslick, Effect of cavitation conditions on amorphous metal synthesis, *Ultrasonics*, 1992, **30**, 168–172.

56 T. Hyeon, M. Fang and K. S. Suslick, Nanostructured molybdenum carbide: sonochemical synthesis and catalytic properties, *J. Am. Chem. Soc.*, 1996, **118**, 5492–5493.

57 C. Cau and S. I. Nikitenko, Mechanism of $W(CO)_6$ sonolysis in diphenylmethane, *Ultrason. Sonochem.*, 2012, **19**, 498–502.

58 Y. Koltypin, X. Cao, R. Prozorov, J. Balogh, D. Kaptas and A. Gedanken, Sonochemical synthesis of iron nitride nanoparticles, *J. Mater. Chem.*, 1997, **7**, 2453–2456.

59 P. M. Sakkas, C. Bozes, D. G. Kanellopoulou, G. Sourkouni and C. Argirusis, A study on the synchronous decoration of molybdenum oxide or tungsten oxide nanoparticles on anode materials for natural gas fed solid oxide fuel cells using ultrasounds, *Ultrason. Sonochem.*, 2019, **59**, 104715.

60 A. I. Argüelles-Pesqueira, N. M. Diéguez-Armenta, A. K. Bobadilla-Valencia, S. K. Nataraj, A. Rosas-Durazo, R. Esquivel, M. E. Alvarez-Ramos, R. Escudero, P. Guerrero-German, J. A. Lucero-Acuña and P. Zavala-Rivera, Low intensity sonosynthesis of iron carbide@iron oxide core-shell nanoparticles, *Ultrason. Sonochem.*, 2018, **49**, 303–309.

61 K. S. Suslick, M. Fang and T. Hyeon, Sonochemical synthesis of iron colloids, *J. Am. Chem. Soc.*, 1996, **118**, 11960–11961.

62 S. I. Nikitenko, Y. Koltypin, O. Palchik, I. Felner, X. N. Xu and A. Gedanken, Synthesis of Highly Magnetic, Air-stable iron-iron carbide nanocrystalline particles by using power ultrasound, *Angew. Chem., Int. Ed.*, 2001, **40**, 4447.

63 M. M. Mdleleni, T. Hyeon and K. S. Suslick, Sonochemical synthesis of nanostructured molybdenum sulfide, *J. Am. Chem. Soc.*, 1998, **120**, 6189–6190.

64 L. H. Abdel-Rahman, A. M. Abu-Dief, R. M. El-Khatib and S. M. Abdel-Fatah, Sonochemical synthesis, DNA binding, antimicrobial evaluation and *in vitro* anticancer activity of three new nano-sized Cu(II), Co(II) and Ni(II) chelates based on tri-dentate NOO imine ligands as precursors for metal oxides, *J. Photochem. Photobiol., B*, 2016, **162**, 298–308.

65 A. M. Elseman, D. A. Rayan and M. M. Rashad, Structure, optical and magnetic behavior of nanocrystalline CuO nanopowders synthesized *via* a new technique using Schiff base complex, *J. Mater. Sci.: Mater. Electron.*, 2016, **27**, 2652–2661.

66 M. K. Mohammadi, P. Hayati, S. Jafari, M. Karimi and A. Gutierrez, Sonication-assisted synthesis of a new rod-like metal-organic coordination polymer compound; novel precursor to produce pure phase nano-sized lead(II) oxide, *J. Mol. Struct.*, 2019, **1176**, 434–446.

67 V. B. Kumar, I. Perelshtein, A. Lipovsky, Z. Porat and A. Gedanken, The sonochemical synthesis of Ga@C-dots particles, *RSC Adv.*, 2015, **5**, 25533–25540.

68 V. B. Kumar, M. Monte, O. Mathon, S. Pascarelli, Z. Porat and A. Gedanken, The interaction between molten gallium and the hydrocarbon medium induced by ultrasonic energy–can gallium carbide be formed?, *J. Am. Ceram. Soc.*, 2017, **100**, 3305–3315.

69 N. A. Dhas and K. S. Suslick, Sonochemical preparation of hollow nanospheres and hollow nanocrystals, *J. Am. Chem. Soc.*, 2005, **127**, 2368–2369.

70 N. Du, H. Zhang, B. D. Chen, J. B. Wu, X. Y. Ma, Z. H. Liu, Y. Q. Zhang, D. R. Yang, X. H. Huang and J. P. Tu, Porous $Co_3O_4$ nanotubes derived from $Co_4(CO)_{12}$ clusters on carbon nanotube templates: a highly efficient material for Li-Battery applications, *Adv. Mater.*, 2007, **19**, 4505–4509.

71 J. H. Bang and K. S. Suslick, Sonochemical synthesis of nanosized hollow hematite, *J. Am. Chem. Soc.*, 2007, **129**, 2242–2243.

72 A. P. C. Bedini, B. Klingebiel, M. Luysberg and R. Carius, Sonochemical synthesis of hydrogenated amorphous silicon nanoparticles from liquid trisilane at ambient temperature and pressure, *Ultrason. Sonochem.*, 2017, **39**, 883–888.

73 B. T. Mayers, K. Liu, D. Sunderland and Y. N. Xia, Sonochemical synthesis of trigonal selenium nanowires, *Chem. Mater.*, 2003, **15**, 3852–3858.

74 S. H. Jeong, J. H. Ko, J. B. Park and W. Park, A sonochemical route to single-walled carbon nanotubes under ambient conditions, *J. Am. Chem. Soc.*, 2004, **126**, 15982–15983.

75 S. Barcikowski, A. Plech, K. S. Suslick and A. Vogel, Materials synthesis in a bubble, *MRS Bull.*, 2019, **44**, 382–391.

76 M. Lu and L. Zhou, One-step sonochemical synthesis of versatile nitrogen-doped carbon quantum dots for sensitive detection of $Fe^{2+}$ ions and temperature *in vitro*, *Mater. Sci. Eng., C*, 2019, **101**, 352–359.

77 D. G. Shchukin, E. Skorb, V. Belova and H. Moehwald, Ultrasonic cavitation at solid surfaces, *Adv. Mater.*, 2011, **23**, 1922–1934.

78 K. Okitsu, M. Ashokkumar and F. Grieser, Sonochemical synthesis of gold nanoparticles: effects of ultrasound frequency, *J. Phys. Chem. B*, 2005, **109**, 20673–20675.

79 K. Okitsu, K. Sharyo and R. Nishimura, One-pot synthesis of gold nanorods by ultrasonic irradiation: the effect of pH on the shape of the gold nanorods and nanoparticles, *Langmuir*, 2009, **25**, 7786–7790.

80 A. Sánchez-Iglesias, I. Pastoriza-Santos, J. Pérez-Juste, B. Rodríguez-González, F. J. García de Abajo and

L. M. Liz-Marzán, Synthesis and optical properties of gold nanodecahedra with size control, *Adv. Mater.*, 2006, **18**, 2529–2534.

81 J. Zhang, J. Du, B. Han, Z. Liu, T. Jiang and Z. Zhang, Sonochemical formation of single-crystalline gold nanobelts, *Angew. Chem., Int. Ed.*, 2006, **45**, 1116–1119.

82 L. P. Jiang, S. Xu, J. M. Zhu, J. R. Zhang, J. J. Zhu and H. Y. Chen, Ultrasonic-assisted synthesis of monodisperse single-crystalline silver nanoplates and gold nanorings, *Inorg. Chem.*, 2004, **43**, 5877–5883.

83 P. Zhang, J. He, X. Ma, J. Gong and Z. Nie, Ultrasound assisted interfacial synthesis of gold nanocones, *Chem. Commun.*, 2013, **49**, 987–989.

84 Y. Mizukoshi, K. Okitsu, Y. Maeda, T. A. Yamamoto, R. Oshima and Y. Nagata, Sonochemical preparation of bimetallic nanoparticles of gold/palladium in aqueous solution, *J. Phys. Chem. B*, 1997, **101**, 7033–7037.

85 S. Anandan, F. Grieser and M. Ashokkumar, Sonochemical synthesis of Au-Ag core-shell bimetallic nanoparticles, *J. Phys. Chem. C*, 2008, **112**, 15102–15105.

86 H. Ataee-Esfahani, L. Wang, Y. Nemoto and Y. Yamauchi, Synthesis of bimetallic Au@Pt nanoparticles with Au core and nanostructured Pt shell toward highly active electrocatalysts, *Chem. Mater.*, 2010, **22**, 6310–6318.

87 C. Gümeci, D. U. Cearnaigh, D. J. Casadonte and C. Korzeniewski, Synthesis of $PtCu_3$ bimetallic nanoparticles as oxygen reduction catalysts *via* a sonochemical method, *J. Mater. Chem. A*, 2013, **1**, 2322–2329.

88 A. Godínez-García, J. F. Pérez-Robles, H. V. Martínez-Tejada and O. Solorza-Feria, Characterization and electrocatalytic properties of sonochemical synthesized PdAg nanoparticles, *Mater. Chem. Phys.*, 2012, **134**, 1013–1019.

89 M. A. Matin, J. H. Jang and Y. U. Kwon, PdM nanoparticles (M=Ni, Co, Fe, Mn) with high activity and stability in formic acid oxidation synthesized by sonochemical reactions, *J. Power Sources*, 2014, **262**, 356–363.

90 J. Li, C. J. Ke, C. Lin, Z. H. Cai, C. Y. Chen and W. H. Chang, Facile method for gold nanocluster synthesis and fluorescence control using toluene and ultrasound, *J. Med. Biol. Eng.*, 2013, **33**, 23–28.

91 H. Xu and K. S. Suslick, Sonochemical synthesis of highly fluorescent Ag nanoclusters, *ACS Nano*, 2010, **4**, 3209–3214.

92 T. Liu, L. Zhang, H. Song, Z. Wang and Y. Lv, Sonochemical synthesis of Ag nanoclusters: electrogenerated chemiluminescence determination of dopamine, *Luminescence*, 2013, **28**, 530–535.

93 T. Zhou, M. Rong, Z. Cai, C. J. Yang and X. Chen, Sonochemical synthesis of highly fluorescent glutathione-stabilized Ag nanoclusters and $S^{2-}$ sensing, *Nanoscale*, 2012, **4**, 4103–4106.

94 C. Wang, H. Cheng, Y. Huang, Z. Xu, H. Lin and C. Zhang, Facile sonochemical synthesis of pH-responsive copper nanoclusters for selective and sensitive detection of $Pb^{2+}$ in living cells, *Analyst*, 2015, **140**, 5634–5639.

95 M. Yildirim, A. S. Kipcak and E. M. Derun, Sonochemical-assisted magnesium borate synthesis from different boron sources, *Pol. J. Chem. Technol.*, 2017, **19**, 81–88.

96 I. Doroshenko, J. Zurkova, Z. Moravec, P. Bezdicka and J. Pinkas, Sonochemical precipitation of amorphous uranium phosphates, from trialkyl phosphate solutions and their thermal conversion to $UP_2O_7$, *Ultrason. Sonochem.*, 2015, **26**, 157–162.

97 T. T. T. Le, T. V. Vu, H. Kim, D. Jeong, B. Pejjai, N. T. N. Truong and C. Park, Green and low-cost synthesis of CIGSe nanoparticles using ethanol as a solvent by a sonochemical method-A new approach, *Mater. Chem. Phys.*, 2018, **207**, 522–529.

98 D. Chen, S. H. Yoo, Q. Huang, G. Ali and S. O. Cho, Sonochemical synthesis of Ag/AgCl nanocubes and their efficient visible-light-driven photocatalytic performance, *Chem.–Eur. J.*, 2012, **18**, 5192–5200.

99 F. Xu, Y. Yuan, H. Han, D. Wu, Z. Gao and K. Jiang, Synthesis of ZnO/CdS hierarchical heterostructure with enhanced photocatalytic efficiency under nature sunlight, *CrystEngComm*, 2012, **14**, 3615–3622.

100 M. Abbasa, W. Tawfik and J. Chen, CdO nanorods and $Cd(OH)_2$/Ag core/satellite nanorods: Rapid and efficient sonochemical synthesis, characterization and their magnetic properties, *Ultrason. Sonochem.*, 2018, **40**, 577–582.

101 R. L. Palomino, A. M. B. Miró, F. N. Tenorio, F. S. D. Jesús, C. A. C. Escobedo and S. Ammar, Sonochemical assisted synthesis of $SrFe_{12}O_{19}$ nanoparticles, *Ultrason. Sonochem.*, 2016, **29**, 470–475.

102 R. L. P. Resendiz, F. S. D. Jesús, C. A. C. Escobedo, L. E. H. Cruz and A. M. B. Miró, Effect of sonication output power on the crystal structure and magnetism of $SrFe_{12}O_{19}$ nanoparticles, *Crystals*, 2018, **8**, 45.

103 E. L. S. Souza, J. C. Sczancoski, I. C. Nogueira, M. A. P. Almeida, M. O. Orlandi, M. S. Li, R. A. S. Luz, M. G. R. Filho, E. Longo and L. S. Cavalcante, Structural evolution, growth mechanism and photoluminescence properties of $CuWO_4$ nanocrystals, *Ultrason. Sonochem.*, 2017, **38**, 256–270.

104 C. Cau, Y. Guari, T. Chave, J. Larionova, P. Pochon and S. I. Nikitenko, Sonohydrothermal synthesis of nanostructured $(Ce,Zr)O_2$ mixed oxides with enhanced catalytic performance, *J. Phys. Chem. C*, 2013, **117**, 22827–22833.

105 S. I. Nikitenko, T. Chave, C. Cau, H. Brau and V. Flaud, Photothermal hydrogen production using noble-metal-free $Ti@TiO_2$ core-shell nanoparticles under visible-NIR light irradiation, *ACS Catal.*, 2015, **5**, 4790–4795.

106 M. Gancheva, M. Markova-Velichkova, G. Atanasova, D. Kovacheva, I. Uzunov and R. Cukeva, Design and photocatalytic activity of nanosized zinc oxides, *Appl. Surf. Sci.*, 2016, **368**, 258–266.

107 A. Moghtada and R. Ashiri, Superiority of sonochemical processing method for the synthesis of barium titanate nanocrystals in contrast to the mechanochemical approach, *Ultrason. Sonochem.*, 2018, **41**, 127–133.

108 J. Zhu, S. Xu, H. Wang, J. Zhu and H. Chen, Sonochemical synthesis of CdSe hollow spherical assemblies *via* an *in situ* template route, *Adv. Mater.*, 2003, **15**, 156–159.

109 P. K. Vabbina, A. Kaushik, N. Pokhrel, S. Bhansali and N. Pala, Electrochemical cortisol immunosensors based on sonochemically synthesized zinc oxide 1D nanorods and 2D nanoflakes, *Biosens. Bioelectron.*, 2015, **63**, 124–130.

110 J. Geng, J. Zhu, D. Lu and H. Chen, Hollow $PbWO_4$ nanospindles *via* a facile sonochemical route, *Inorg. Chem.*, 2006, **45**, 8403–8407.

111 J. M. Rankin, N. K. Neelakantan, K. E. Lundberg, E. M. Grzincic, C. J. Murphy and K. S. Suslick, Magnetic, fluorescent, and copolymeric silicone microspheres, *Adv. Sci.*, 2015, **2**, 6.

112 A. K. P. Mann, S. Wicker and S. E. Skrabalak, Aerosol-assisted molten salt synthesis of $NaInS_2$ nanoplates for use as a new photoanode material, *Adv. Mater.*, 2012, **24**, 6186–6191.

113 Y. Zhang, L. A. Huff, A. A. Gewirth and K. S. Suslick, Synthesis of manganese oxide microspheres by ultrasonic spray pyrolysis and their application as supercapacitors, *Part. Part. Syst. Charact.*, 2015, **32**, 899–906.

114 K. Muthoosamy and S. Manickam, State of the art and recent advances in the ultrasound-assisted synthesis, exfoliation and functionalization of graphene derivatives, *Ultrason. Sonochem.*, 2017, **39**, 478–493.

115 Z. Wu, W. Ren, L. Gao, B. Liu, J. Zhao and H. Cheng, Efficient synthesis of graphene nanoribbons sonochemically cut from graphene sheets, *Nano Res.*, 2010, **3**, 16–22.

116 D. Li, M. B. Mueller, S. Gilje, R. B. Kaner and G. G. Wallace, Processable aqueous dispersions of graphene nanosheets, *Nat. Nanotechnol.*, 2007, **3**, 101–105.

117 K. Krishnamoorthy, G. Kim and S. J. Kim, Graphene nanosheets: Ultrasound assisted synthesis and characterization, *Ultrason. Sonochem.*, 2013, **20**, 644–649.

118 X. Li, G. Zhang, X. Bai, X. Sui, X. Wang, E. Wang and H. Dai, Highly conducting graphene sheets and Langmuir–Blodgett films, *Nat. Nanotechnol.*, 2008, **3**, 538–542.

119 A. A. Green and M. C. Hersam, Solution phase production of graphene with controlled thickness *via* density differentiation, *Nano Lett.*, 2009, **9**, 4031–4036.

120 Z. Fan, W. Kai, J. Yan, T. Wei, L. Zhi, J. Feng, Y. Ren, L. Song and F. Wei, Facile synthesis of graphene nanosheets *via* Fe reduction of exfoliated graphite oxide, *Acs Nano*, 2011, **5**, 191–198.

121 T. Soltani and B. Lee, Low intensity-ultrasonic irradiation for highly efficient, eco-friendly and fast synthesis of graphene oxide, *Ultrason. Sonochem.*, 2017, **38**, 693–703.

122 H. Yang, H. Li, J. Zhai, L. Sun and H. Yu, Simple synthesis of graphene oxide using ultrasonic cleaner from expanded graphite, *Ind. Eng. Chem. Res.*, 2014, **53**(46), 17878–17883.

123 A. Esmaeili and M. H. Entezari, Facile and fast synthesis of graphene oxide nanosheets *via* bath ultrasonic irradiation, *J. Colloid Interface Sci.*, 2014, **432**, 19–25.

124 A. Abulizi, K. Okitsu and J. Zhu, Ultrasound assisted reduction of graphene oxide to graphene in L-ascorbic acid aqueous solutions: Kinetics and effects of various factors on the rate of graphene formation, *Ultrason. Sonochem.*, 2014, **21**, 1174–1181.

125 T. Soltani and B. Lee, A benign ultrasonic route to reduced graphene oxide from pristine graphite, *J. Colloid Interface Sci.*, 2017, **486**, 337–343.

126 R. G. Bai, K. Muthoosamy, F. N. Shipton and S. Manickam, Acoustic cavitation induced generation of stabilizer-free, extremely stable reduced graphene oxide nanodispersion for efficient delivery of paclitaxel in cancer cells, *Ultrason. Sonochem.*, 2017, **36**, 129–138.

127 H. Naeimia, M. Golestanzadeh and Z. Zahraie, Synthesis of potential antioxidants by synergy of ultrasound andacidic graphene nanosheets as catalyst in water, *Int. J. Biol. Macromol.*, 2016, **83**, 345–357.

128 M. Mirza-Aghayan, M. M. Tavana and R. Boukherroub, Sulfonated reduced graphene oxide as a highly efficient catalyst for direct amidation of carboxylic acids with amines using ultrasonic irradiation, *Ultrason. Sonochem.*, 2016, **29**, 371–379.

129 S. Stankovich, R. D. Piner, S. T. Nguyen and R. S. Ruoff, Synthesis and exfoliation of isocyanate-treated graphene oxide nanoplatelets, *Carbon*, 2006, **44**, 3342–3347.

130 J. Jia, Y. Gai, W. Wang and Y. Zhao, Green synthesis of biocompatiable chitosan-graphene oxide hybrid nanosheet by ultrasonication method, *Ultrason. Sonochem.*, 2016, **32**, 300–306.

131 Y. Hernandez, V. Nicolosi, M. Lotya, F. M. Blighe, Z. Sun, S. De, I. T. McGovern, B. Holland, M. Byrne, Y. K. Gun'Ko, J. J. Boland, P. Niraj, G. Duesberg, S. Krishnamurthy, R. Goodhue, J. Hutchison, V. Scardaci, V. A. C. Ferrari and J. N. Coleman, High-yield production of graphene by liquid-phase exfoliation of graphite, *Nat. Nanotechnol.*, 2008, **3**, 563–568.

132 J. N. Coleman, M. Lotya, A. O'Neill, S. D. Bergin, P. J. King, U. Khan, K. Young, A. Gaucher, S. De, R. J. Smith, I. V. Shvets, S. K. Arora, G. Stanton, H. Y. Kim, K. Lee, G. T. Kim, G. S. Duesberg, T. Hallam, J. J. Boland, J. J. Wang, J. F. Donegan, J. C. Grunlan, G. Moriarty, A. Shmeliov, R. J. Nicholls, J. M. Perkins, E. M. Grieveson, K. Theuwissen, D. W. McComb, P. D. Nellist and V. Nicolosi, Two-dimensional nanosheets produced by liquid exfoliation of layered materials, *Science*, 2011, **331**, 568–571.

133 J. Walter, M. Nishioka and S. Hara, Ultrathin platinum nanoparticles encapsulated in a graphite lattice-prepared by a sonochemical approach, *Chem. Mater.*, 2001, **13**, 1828–1833.

134 J. E. Jones, M. C. Cheshire, D. J. Casadonte and C. C. Phifer, Facile sonochemical synthesis of graphite intercalation compounds, *Org. Lett.*, 2004, **6**, 1915–1917.

135 L. M. Viculis, J. J. Mack and R. B. Kaner, A chemical route to carbon nanoscrolls, *Science*, 2003, **299**, 1361.

136 J. Guo, S. Zhu, Z. Chen, Y. Li, Z. Yu, Q. Liu, J. Li, C. Feng and D. Zhang, Sonochemical synthesis of $TiO_2$ nanoparticles on graphene for use as photocatalyst, *Ultrason. Sonochem.*, 2011, **18**, 1082–1090.

137 Y. Cui, D. Zhou, Z. Sui and B. Han, Sonochemical synthesis of graphene oxide-wrapped gold nanoparticles hybrid materials: visible light photocatalytic activity, *Chin. J. Chem.*, 2014, **33**, 119–124.

138 S. Zhu, J. Guo, J. Dong, Z. Cui, T. Lu, C. Zhu, D. Zhang and J. Ma, Sonochemical fabrication of $Fe_3O_4$ nanoparticles on reduced graphene oxide for biosensors, *Ultrason. Sonochem.*, 2013, **20**, 872–880.

139 H. C. Yau, M. K. Bayazit, J. H. G. Steinke and M. S. P. Shaffer, Sonochemical degradation of nmethylpyrrolidone and its influence on single walled carbon nanotube dispersion, *Chem. Commun.*, 2015, **51**, 16621–16624.

140 H. Ha and S. H. Jeong, Facile route to multi-walled carbon nanotubes under ambient conditions, *Korean J. Chem. Eng.*, 2016, **33**, 401–404.

141 V. B. Kumar, Z. Porat and A. Gedanken, Facile one-step sonochemical synthesis of ultrafine and stable fluorescent C-dots, *Ultrason. Sonochem.*, 2016, **28**, 367–375.

142 K. Wei, J. Li, Z. Ge, Y. You and H. Xu, Sonochemical synthesis of highly photoluminescent carbon nanodots, *RSC Adv.*, 2014, **4**, 52230–52234.

143 I. Nissan, V. B. Kumar, Z. Porat, D. Makove, O. Shefi and A. Gedanken, Sonochemically-fabricated Ga@C-dots@Ga nanoparticle-aided neural growth, *J. Mater. Chem. B*, 2017, **5**, 1371–1379.

144 D. W. Jung, D. A. Yang, J. Kim, J. Kim and W. S. Ahn, Facile synthesis of MOF-177 by a sonochemical method using 1-methyl-2-pyrrolidinone as a solvent, *Dalton Trans.*, 2010, **39**, 2883–2887.

145 D. A. Yang, H. Y. Cho, J. Kim, S. T. Yang and W. S. Ahn, $CO_2$ capture and conversion using Mg-MOF-74 prepared by a sonochemical method, *Energy Environ. Sci.*, 2012, **5**, 6465–6473.

146 A. Mehrani, A. Morsali, Y. Hanifehpour and S. W. Joo, Sonochemical temperature controlled synthesis of pellet-, laminate- and rice grain-like morphologies of a Cu(II) porous metal-organic framework nano-structures, *Ultrason. Sonochem.*, 2014, **21**, 1430–1434.

147 V. Safarifard and A. Morsali, Facile preparation of nanocubes zinc-based metal-organic framework by an ultrasound-assisted synthesis method; precursor for the fabrication of zinc oxide octahedral nanostructures, *Ultrason. Sonochem.*, 2018, **40**, 921–928.

148 S. A. A. Razavi, M. Y. Masoomi and A. Morsali, Morphology-dependent sensing performance of dihydro-tetrazine functionalized MOF toward Al(III), *Ultrason. Sonochem.*, 2018, **41**, 17–26.

149 W. J. Son, J. Kim, J. Kim and W. S. Ahn, Sonochemical synthesis of MOF-5, *Chem. Commun.*, 2008, **47**, 6336–6338.

150 Y. R. Lee, S. M. Cho, W. S. Ahn, C. H. Lee, K. H. Lee and W. S. Cho, Facile synthesis of an IRMOF-3 membrane on porous $Al_2O_3$ substrate *via* a sonochemical route, *Microporous Mesoporous Mater.*, 2015, **213**, 161–168.

151 S. Dharmarathna, C. K. King'ondu, W. Pedrick, L. Pahalagedara and S. L. Suib, Direct sonochemical synthesis of manganese octahedral molecular sieve (OMS-2) nanomaterials using cosolvent systems, their characterization, and catalytic applications, *Chem. Mater.*, 2012, **24**, 705–712.

152 J. A. Thompson, K. W. Chapman, W. J. Koros, C. W. Jones and S. Nair, Sonication-induced ostwald ripening of ZIF-8 nanoparticles and formation of ZIF-8/polymer composite membranes, *Microporous Mesoporous Mater.*, 2012, **158**, 292–299.

153 O. Abuzalat, D. Wong, M. Elsayed, S. Park and S. Kim, Sonochemical fabrication of Cu(II) and Zn(II) metal-organic framework films on metal substrates, *Ultrason. Sonochem.*, 2018, **45**, 180–188.

154 H. M. Xiong, D. G. Shchukin, H. Moehwald, Y. Xu and Y. Y. Xia, Sonochemical synthesis of highly luminescent zinc oxide nanoparticles doped with magnesium(II), *Angew. Chem., Int. Ed.*, 2009, **48**, 2727–2731.

155 V. Belova, T. Borodina, H. Moehwald and D. G. Shchukin, The effect of high intensity ultrasound on the loading of Au nanoparticles into titanium dioxide, *Ultrason. Sonochem.*, 2011, **18**, 310–317.

156 H. Terraschke, J. Olchowka, E. Geringer, A. V. Rodrigues and C. Wickleder, Facile Ionic liquid-assisted strategy for direct precipitation of $Eu^{2+}$-activated nanophosphors under ambient conditions, *Small*, 2018, **14**, 1703707.

157 K. N. Venkatachalaiaha, H. Nagabhushana, G. P. Darshan, R. B. Basavaraj, B. Daruka Prasad and S. C. Sharma, Structural, morphological and photometric properties of sonochemically synthesized $Eu^{3+}$ doped $Y_2O_3$ nanophosphor for optoelectronic devices, *Mater. Res. Bull.*, 2017, **94**, 442–455.

158 Y. Li, R. Lei and S. Xu, Combination of ionic liquid and sonication: a fast, mild and green way to fabricate Europium-doped lanthanide nanophosphates, *ChemistrySelect*, 2016, **1**, 4861–4867.

159 J. Yu, J. Yu, W. Ho and L. Zhang, Preparation of highly photocatalytic active nano-sized $TiO_2$ particles *via* ultrasonic irradiation, *Chem. Commun.*, 2001, **19**, 1942–1943.

160 P. J. Jodłowski, D. K. Chlebda, R. J. Jedrzejczyk, A. Dziedzicka, Ł. Kuterasinski and M. Sitarz, Characterisation of well-adhered $ZrO_2$ layers produced on structured reactors using the sonochemical sol–gel method, *Appl. Surf. Sci.*, 2018, **427**, 563–574.

161 A. F. Sierra-Salazar, T. Chave, A. Ayral, S. I. Nikitenko, V. Hulea, P. J. Kooyman, F. D. Tichelaar, S. Perathoner and P. Lacroix-Desmazes, Engineering of silica-supported platinum catalysts with hierarchical porosity combining latex synthesis, sonochemistry and sol-gel process–I. Material preparation, *Microporous Mesoporous Mater.*, 2016, **234**, 207–214.

162 A. F. Sierra-Salazar, A. Ayral, T. Chave, V. Hulea, S. I. Nikitenko, S. Perathoner and P. Lacroix-Desmazes, Hierarchical porosity tailoring of sol-gel derived $Pt/SiO_2$ catalysts, *Top. Catal.*, 2018, **61**, 1424–1436.

163 D. Manoharan, A. Loganathan, V. Kurapati and V. J. Nesamony, Unique sharp photoluminescence of size-

 

controlled sonochemically synthesized zirconia nanoparticles, *Ultrason. Sonochem.*, 2015, **23**, 174–184.

164 M. Zhang, M. Chen, Y. Liu, Y. Wang and J. Tang, Catalase-inorganic hybrid microflowers modified glassy carbon electrode for amperometric detection of hydrogen peroxide, *Mater. Lett.*, 2019, **243**, 9–12.

165 B. M. Teo, S. K. Suh, T. A. Hatton, M. Ashokkumar and F. Grieser, Sonochemical synthesis of magnetic janus nanoparticles, *Langmuir*, 2011, **27**, 30–33.

166 Z. Li, X. Du, X. Cui and Z. Wang, Ultrasonic-assisted fabrication and release kinetics of two model redox-responsive magnetic microcapsules for hydrophobic drug delivery, *Ultrason. Sonochem.*, 2019, **57**, 223–232.

167 A. Gedanken, Preparation and properties of proteinaceous microspheres made sonochemically, *Chem.–Eur. J.*, 2008, **14**, 3840–3853.

168 X. Du, Z. Li, J. Xia, F. Zhang and Z. Wang, Facile sonochemistry-assisted assembly of the water-loving drug-loaded micro-organogel with thermo- and redox-sensitive behavior, *Colloids Surf., A*, 2019, **561**, 47–56.

169 T. S. H. Leong, G. J. O. Martin and M. Ashokkumar, Ultrasonic encapsulation-a review, *Ultrason. Sonochem.*, 2017, **35**, 605–614.

170 Z. Li, J. Dong, H. Zhang, Y. Zhang, H. Wang, X. Cui and Z. Wang, Sonochemical catalysis as a unique strategy for the fabrication of nano-/micro-structured inorganics, *Nanoscale Adv.*, 2021, **3**, 41–72.

171 D. Radziuk and H. Moehwald, Ultrasonically treated liquid interfaces for progress in cleaning and separation processes, *Phys. Chem. Chem. Phys.*, 2016, **18**, 21–46.

172 S. He, S. Zhong, L. Xu, Y. Dou, Z. Li, F. Qiao, Y. Gao and X. Cui, Sonochemical fabrication of magnetic reduction-responsive alginatebased microcapsules for drug delivery, *Int. J. Biol. Macromol.*, 2020, **155**, 42–49.

173 Y. Sun, C. Shi, J. Yang, S. Zhong, Z. Li, L. Xu, S. Zhao, Y. Gao and X. Cui, Fabrication of folic acid decorated reductive-responsive starch-based microcapsules for targeted drug delivery *via* sonochemical method, *Carbohydr. Polym.*, 2018, **200**, 508–515.